

Experimental Search for a Bound (Σ^-n) Dibaryon State*

HOWARD F. DAVIS† AND H. RICHARD GUSTAFSON‡

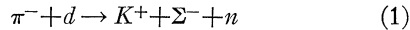
University of Washington, Seattle, Washington 98105

(Received 26 May 1969)

An experimental search for a bound (Σ^-n) state produced an upper limit on the $\pi^-+d \rightarrow K^++(\Sigma^-n)$ cross section. For $P_{\pi^- \text{lab}} = 1.15 \text{ GeV}/c$, $25^\circ \lesssim \theta_{K^+ \text{lab}} \lesssim 60^\circ$, and an experimental width of $\pm 10 \text{ MeV}$ in the (Σ^-n) mass, the result is $\sigma \leq 0.16 \mu\text{b sr}^{-1}$, 90% confidence. This limit on the (Σ^-n) production cross section is compared with the prediction of the Henley-Dante impulse model for 1S_0 (Σ^-n) production; this comparison leads to an upper limit on the 1S_0 (Σ^-n) binding energy of 0.3 MeV, 90% confidence limit.

I. INTRODUCTION

AN experimental search for a (Σ^-n) bound state was designed, run at the Cosmotron, and analyzed. The analyzed data collected on the reaction



at $P_\pi \sim 1.15 \text{ GeV}/c$, are used to give an upper limit on the 1S_0 (Σ^-n) state's possible binding energy (BE).¹ The small upper limit on the BE of 0.3 MeV makes it improbable, though still possible, that the 1S_0 (Σ^-n) state exist as a bound state.

Among the fundamental octet of baryons [N, Λ, Σ, Ξ],² the dibaryon state (Σ^-n) has the useful property that its discrete quantum numbers are $I = \frac{3}{2}$, $I_z = -\frac{3}{2}$, $Y = 1$, and $B = 2$. A study of its properties is a study of a pure $I = \frac{3}{2}$ dibaryon system.³ The study of the (Σ^-n)⁴ has an advantage over the study of the charge conjugate state, the (Σ^+p) state.⁵ The Coulomb repulsion in the latter's state could preclude it from actually being bound.

The (Σ^-n) state cannot be simply studied in elastic scattering. Even if it could, that would not be the ideal way to search for a bound state. In fact, to reveal a (Σ^-n) bound state and not possibly just a scattering length of a sign consistent with binding, the most direct approach is to try to produce the (Σ^-n) state. Reaction (1) was used to search for the (Σ^-n) bound

state. A quantitative interpretation of (1) is based on a model of final-state hyperon-nucleon interactions.⁶

The experiment based on reaction (1) measured the following quantities: (1) the pion beam momentum and pion beam trajectory through the liquid target; (2) the produced kaon's direction from the liquid target and its range (energy). From these measured quantities with each topologically acceptable event, the invariant mass of the (Σ^-n) system, $M(\Sigma^-n)$, is calculated. This whole set of events constitutes the experimental determination of the cross section $d\sigma/dM(\Sigma^-n)$ near the possible bound (Σ^-n) state; at zero binding energy this mass is simply

$$M_0(\Sigma^-n) = m_{\Sigma^-} + m_n = 2137 \text{ MeV}.$$

The calibration of the experiment's detector system mass scale and resolution was effected through the analysis of the hydrogen-target data from



at $p \sim 1.4 \text{ GeV}/c$.

A statistical sample of 211 events of reaction (1) with $M(\Sigma^-n)$ near $M_0(\Sigma^-n)$, reduced from an initial set of 70 000 pictures, comprised the basic data of the experiment. The detector system and the data are the subject of Secs. II and III. A detailed analysis of the detector system's efficiency, background, and the final analyzed data are the subject of Secs. IV-VI. The conclusions are presented in Sec. VII.

II. EXPERIMENT

The goal was to produce the possible (Σ^-n) bound-particle state using reaction (1) at $p \sim 1.15 \text{ GeV}/c$. An experiment was designed to detect the formation of a (Σ^-n) bound particle indirectly, because of the relatively short life of the Σ^- [$\Gamma(\Sigma^- \rightarrow n + \pi^-) \sim 0.6 \times 10^{10} \text{ sec}^{-1}$] and the anticipated short life of the (Σ^-n) bound particle. By measuring the pion momentum p_π and the kaon range (energy) and direction, KE_K and $\theta_{K\pi}$, we determine the (Σ^-n) invariant mass. The calibration of the mass scale of the detector system was effected by measuring the Σ^- invariant mass in reaction (2).

⁶ E. M. Henley, Phys. Rev. **106**, 1083 (1957); A. Pais and S. B. Treiman, *ibid.* **107**, 1396 (1957); W. M. Dante and E. M. Henley, *ibid.* **144**, 1343 (1965).

* Supported in part by the National Science Foundation.

† Now at Oregon State University, Corvallis, Ore. 97331.

‡ Now at University of Michigan, Ann Arbor, Mich. 48104.

¹ H. F. Davis, H. R. Gustafson, and R. W. Williams, Bull. Am. Phys. Soc. **10**, 702 (1965); H. F. Davis and H. R. Gustafson, *ibid.* **12**, 104 (1967).

² R. J. Oakes, Phys. Rev. **131**, 2239 (1963); S. Iwao, Nuovo Cimento **34**, 1164 (1964).

³ R. H. Dalitz, in *Proceedings of Rutherford Jubilee International Conference, Manchester, 1961*, edited by J. B. Birks (Heywood, London, 1962); R. C. Herndon, Y. C. Tang, and E. W. Schmidt, Phys. Rev. **128**, 2810 (1962); R. H. Dalitz, in *Proceedings of the Oxford International Conference on Elementary Particles, 1965* (Rutherford High Energy Laboratory, Chilton, Berkshire, England, 1966); Y. C. Tang and R. C. Herndon, Phys. Rev. **151**, 1116 (1966); G. Alexander and U. Karshon, in *Proceedings of the Second International Conference on High-Energy Physics and Nuclear Structure, 1967*, edited by G. Alexander (North-Holland, Amsterdam, 1968).

⁴ O. Dahl, N. Horwitz, D. Miller, and J. Murray, Phys. Rev. Letters **4**, 428 (1960); UCRL Report No. UCRL 10348, 1962 (unpublished); T. B. Day, G. A. Snow, and J. Sucher, Phys. Rev. Letters **3**, 61 (1959).

⁵ H. G. Dosch and V. F. Muller, Phys. Letters **19**, 320 (1965); H. G. Dosch, R. Enggelmann, H. Filthuth, V. Hepp, and E. Klunge, *ibid.* **21**, 236 (1966).

Experimentally, a (Σ^-n) bound state would manifest itself in two qualitatively different ways. A large binding energy $BE \gtrsim 50 \text{ MeV} \gg \Delta E$ (ΔE equals the resolution of the detector system), would be apparent as a "line" below the (Σ^-n) invariant mass for the free three-body state of reaction (1). A smaller binding energy $\Delta E \lesssim BE < 0$ would be apparent as an "edge" on the cross section $d\sigma/dM(\Sigma^-n)$. Data were collected in the mass range corresponding to $M_0(\Sigma^-n) - 100 \text{ MeV}$ to $M_0(\Sigma^-n) + 150 \text{ MeV}$.

The identification of a positive kaon stopping in the kaon telescope was the criterion used to establish that reaction (1) was produced. That this is a useful criterion is seen from examining the kinematics. Additional pions could not be produced at $1.15 \text{ GeV}/c$; near $M_0(\Sigma^-n)$, where we are looking for the (Σ^-n), they have no effect. If a positive kaon is identified as having been produced, only a Σ^- and a neutron can have been produced, because of conservation of energy. There are several experimental background effects; these are discussed in Sec. V.

The relative purity of the data from experimental backgrounds was achieved with the use of a thin-window liquid-deuterium target and a measurement, event by event of the pion momentum in a single-magnet momentum spectrometer.

Thus, the principal parts to the experimental method involved, first, the indirect determination of the (Σ^-n) invariant mass and the calibration of the mass scale using reaction (2); secondly, knowing reaction (1) occurred resulted from the identification of the positive kaon.

The experimental techniques of the pion beam and the liquid-deuterium target, the triggering systems, and the spark-chamber systems are described in the following subsections.

A. Particle Beams and Targets

External Proton Beam

The Cosmotron accelerated its internal proton beam to 2.1 GeV and using the Piccioni extraction technique brought out $\sim 15\%$ of this beam into a three-element transport system. This external proton beam was focused and positioned on the $6 \times 1 \times 1$ -in. copper target. The profile of this beam was elliptical in shape, centered on the 1×1 -in. copper; it was about $1\frac{1}{4}$ in. high and 1 in. wide as measured by direct exposure of a sheet of Polaroid film with one pulse at $\sim 1/50$ full beam (see Fig. 1).

The internal proton beam pulses, typically 2×10^{11} protons, were produced at about the rate of 15–20 per minute. Each pulse was spread as uniformly as possible, with no rf structure, over 0.25–0.35 seconds. The resulting beam pion flux per pulse at the liquid target varied between 0.7×10^5 and 2×10^5 , depending on the reproducibility of the system from the extraction mechanism to the pion-beam transport system.

Secondary Negative-Pion Beam

The pion-beam transport system is illustrated in schematic form in Fig. 1. The designed magnification of the system, from copper "pion-producing target" to the liquid target, was 1:1 in the evaluation view and

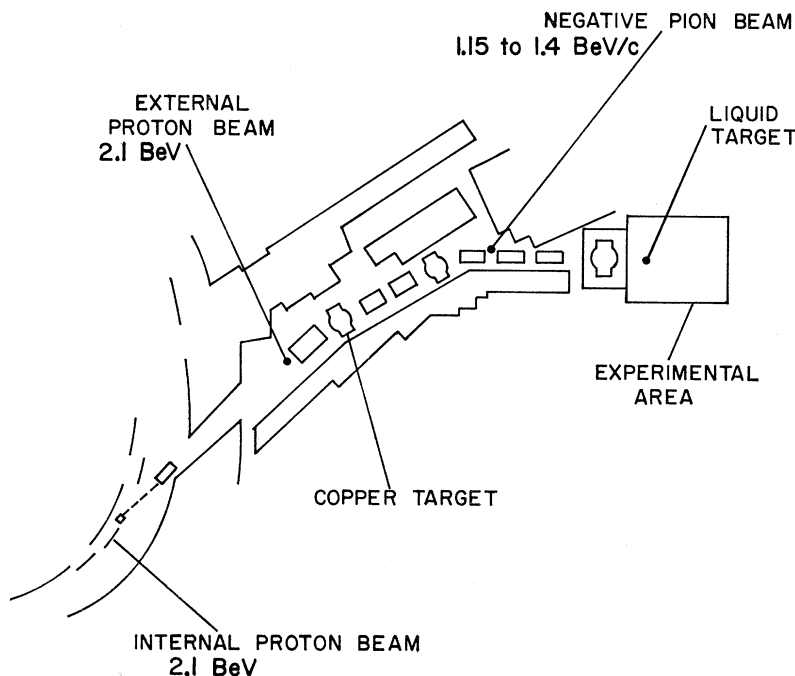


FIG. 1. Particle beams. The plan view of the Cosmotron's external 2.1-GeV proton beam and the secondary negative-pion beam.

1:2 in the plane view. The elevation-view magnification was realized approximately; however, owing to dispersion, the plane-view magnification was somewhat larger than the designed 1:2. We are indebted to the beam design program of Baker, which proved to be a very good start toward the construction of our pion beam, and the designed beam work of Williams. Attempts were made to improve the pion beam and the momentum resolution by putting vertical slits at the approximate horizontal foci; there was little, if any, change in the beam at the hydrogen target other than a change in the number of pions per proton.

The pion beam profile is shown in Fig. 2. The momentum spread was about $\pm 7\%$. The number of pion beam coincident events into the first pair of beam counters was about three times the number of pions incident on the liquid target. The beam composition was π^- , μ^- , and e^- . By making a simple range measurement in lead it was established that less than 5% of the particles at the liquid target were μ^- . The μ^- , e^- component of the beam at the hydrogen target was less than 8%, as determined from the measured μ^- component and the $\mu \rightarrow e$ source of electrons.

B. Negative Pion Beam at Liquid Target

The liquid target is shown in Fig. 2. The target flask was a Mylar cylinder 4 in. in diameter and 20 in. long, surrounded by a radiation shield of aluminized Mylar in the vacuum jacket surrounding the flask. The flask was filled from a closed gas system by cooling the line between the gas cylinders and the flask with liquid hydrogen. This closed system was used to allow the running of target full and target empty without venting the deuterium gas. The gas cylinders were either hydrogen or deuterium, depending on the nature of the data. The level of liquid in the flask was determined by a small pair of resistors in the top of the flask. This did not always prove to be a reliable measure of a full flask. It was necessary to "top off" the target periodically. The target flask was emptied by letting the liquid-hydrogen jacket boil off its contents and thus letting the flask contents escape back to their storage bottles. Simply monitoring the quantity (pions in beam)/(charged particles into kaon telescope) to 1% accuracy proved to be a very good monitor on the liquid target level. The density of the liquid hydrogen, 0.0702 g cm^{-2} , was greater than 50 times the density of the target-empty gaseous hydrogen. The effective transmission thickness of the liquid-hydrogen target was $\sim 1.4 \text{ g cm}^{-2}$.

C. Triggering Detector Systems

Pion Beam and Kaon-Telescope Triggering Systems

The detector arrays are shown in Fig. 3. Five scintillation counters were used to detect the beam pions (π_1 , π_2 , π_3 , π_4 , and π_5). These established that a

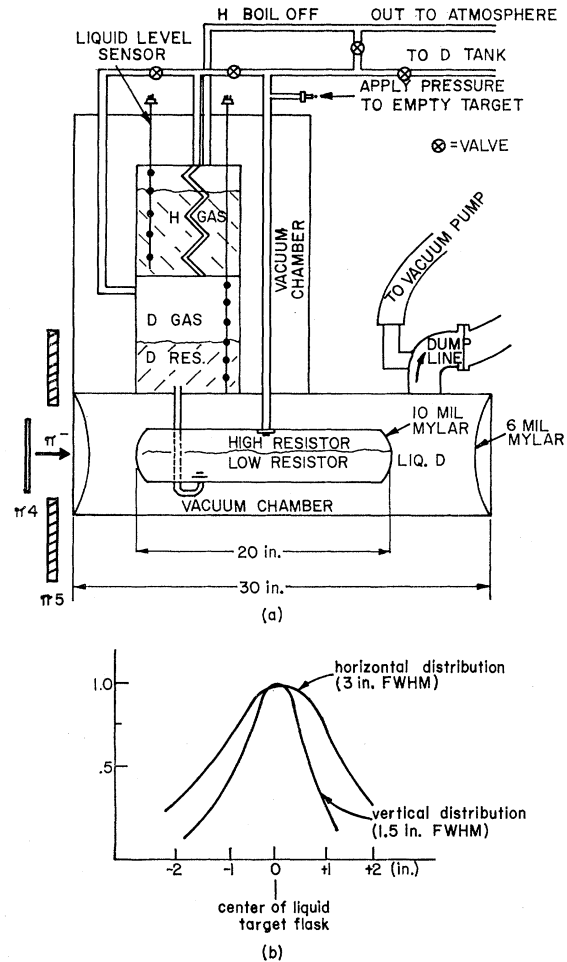


FIG. 2. Negative-pion beam and the liquid target; (a) the liquid target with the last of the pion beam detectors, the target flask and its adjacent heavy walls, and the first of the kaon detectors; (b) a profile of the pion beam where it was incident on the liquid target.

pion passed through the momentum spectrometer and into the liquid target without being coincident with a particle in a 2-in.-wide annular ring directly in front of the liquid target. The dimensions and properties of these counters are in Table I.

There were six scintillation counters in the K telescope: S_1 , S_2 , S_3 , S_4 , S_3' , and S_4' (see Fig. 4). They were all "paddle" shaped with increasing geometrical area and were positioned perpendicular to a line 45° to the direction of the incident pions. All of them were about 0.5 in. thick except S_4' , which was composed of two parallel detectors, fanned in electronically, each 2.0 in. thick.

There were six threshold-type Čerenkov detectors (C_1 , C_2 , C_3 , C_4 , C_5 , and C_6). The first one, C_1 , was one body; the rest were composed of a pair of physical detectors side-by-side fanned in electronically to form one effective detector. The first Čerenkov detector was

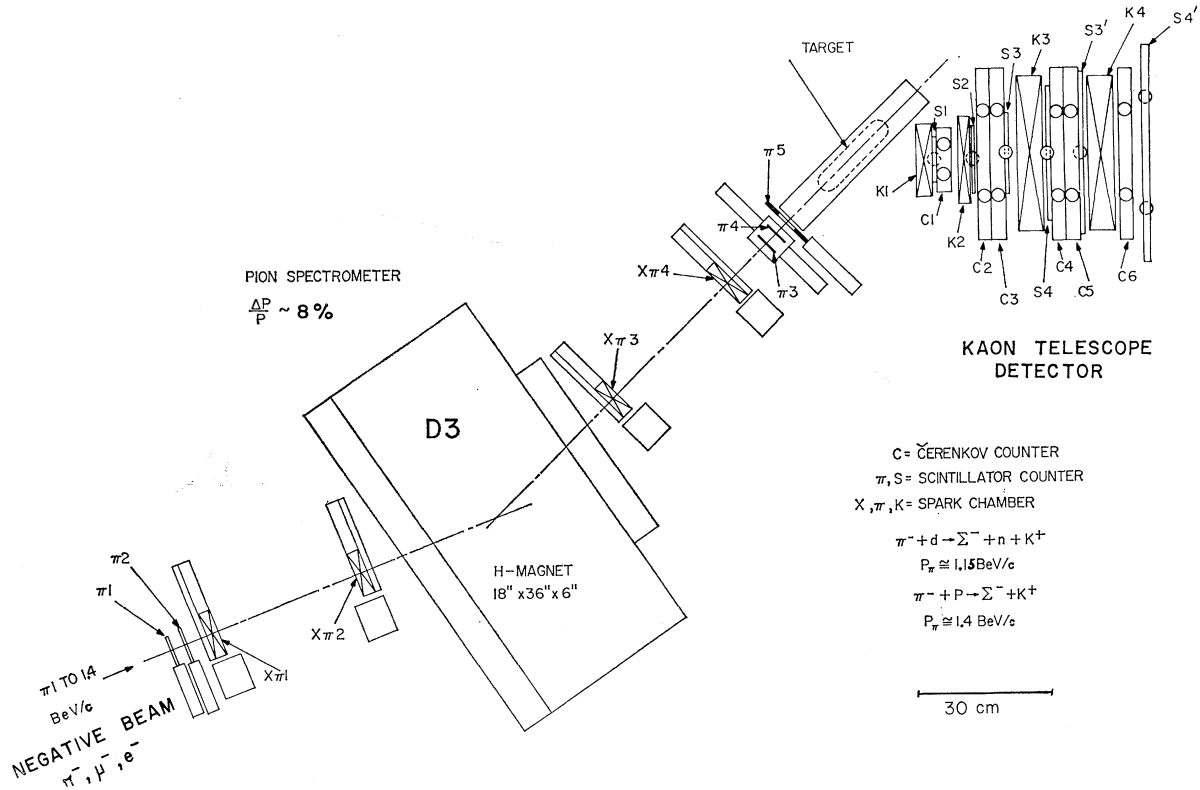


FIG. 3. Triggering counters in the negative-pion beam and in the K telescope. The figure shows the set of counters upstream and downstream of the momentum-spectrometer magnet. The counter furthest downstream is just in front of the liquid target's vacuum window. The figure also shows the spark chambers in the negative-pion beam. These chambers, in conjunction with the magnet, constituted the momentum spectrometer. The chamber furthest downstream was located near the front of the liquid target.

used as a veto to suppress the number of pions that can register as stopped particles in the telescope. All of the other Čerenkov detectors were in coincidence with each other or with a scintillation counter to detect the

TABLE I. Pion beam detectors. (a) Scintillation detectors and (b) spark chambers.

Name	Thickness to beam (in.)	(g/cm ²)	Logical function	Comment
(a) Scintillation detectors				
$\pi 1$	0.38	1	YES	NE102 scintillator
$\pi 2$	0.38	1	YES	NE102 scintillator
$\pi 3$	0.13	0.3	YES	NE102 scintillator and air light coupling
$\pi 4$	0.13	0.3	YES	NE102 scintillator and air light coupling
$\pi 5$	0.5	1.3	NO	NE102 scintillator, annular ring shape
(b) Six-gap foil spark chambers				
Name	Thickness to beam (in.)	(g/cm ²)	Function	
	[$\frac{1}{4}$ -in. gaps and Ne/He (0.95/0.05) gas]			
$X\pi 1$	0.009	0.062 (Al)	} π direction upstream of magnet	
$X\pi 2$	0.009	0.062		
$X\pi 3$	0.009	0.062	} π direction downstream of magnet	
$X\pi 4$	0.009	0.062		

delayed μ^+ through the $K_{\mu 2^+} \rightarrow \mu^+ + \nu_{\mu}$ decay mode; because they were Čerenkov detectors, they were not sensitive to the stopping kaon.

As indicated in Fig. 4, the "S counters" defined the solid angle of the K telescope relative to the liquid target. The K telescope was divided into three sections (K_I , K_{II} , and K_{III}), corresponding to the increasing average depths of penetration of the stopped kaon. The first section, K_I , corresponding to a kaon passing at least through S_3 but not into S_4 . The second section, K_{II} , corresponded to a kaon passing at least through S_4 , but not into S_3' . The third section corresponded to a kaon penetrating to at least S_3' but not to S_4' . The geometrical average solid angle of the sections K_I , K_{II} , and K_{III} are, respectively, ~ 0.2 , ~ 0.15 , and ~ 0.1 sr.

The three sections of the K telescope where the kaons were brought to rest also constituted the three "decay regions" of the K telescope. The pairs of counters C_2C_3 , C_4C_5 , and C_5S_3' comprise the upstream and downstream counters that naturally would "see" the μ^+ of the $K_{\mu 2^+} \rightarrow \mu^+ + \nu_{\mu}$ from region K_I . Similarly the pairs of counters C_4C_5 and C_5S_3' see decays from K_I and the pairs of counters C_4C_5 , C_5S_3' and C_6S_4' see decays from K_{II} . The average geometrical decay solid angles of these decay counters for seeing a $K^+ \rightarrow \mu^+$

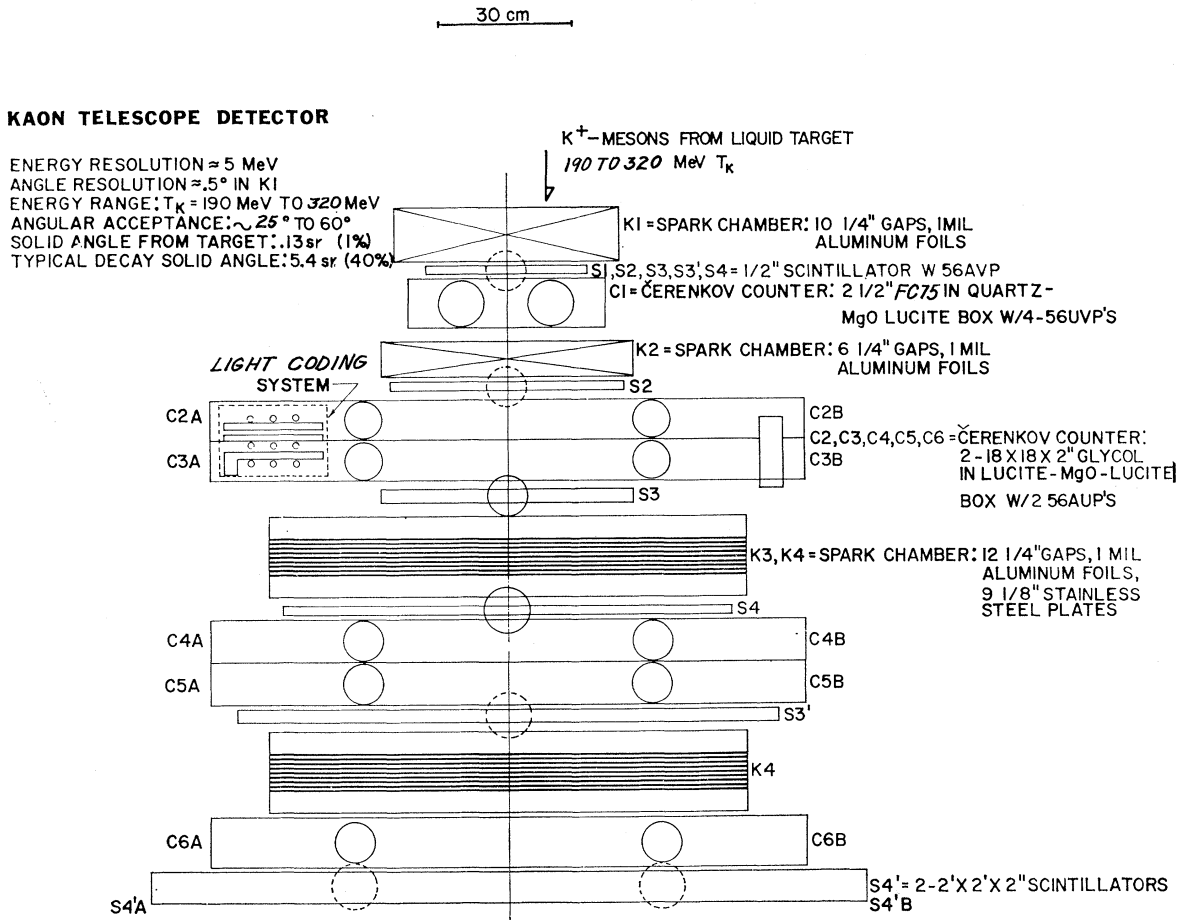


FIG. 4. K telescope. (a) Triggering counters for positive-kaon detection. The first counter, a yes counter, is located at the side of the liquid target near the vacuum window (see Fig. 3). The last counter is positioned at the back of the whole set and is used as a no counter. This figure also shows the spark chambers in the kaon detector. The first and second are 1-mil Al-foil⁷ chambers used to establish the kaon's direction. The second and third are combination 1-mil Al foil chambers and $1/8$ -in. stainless-steel chambers. The latter chambers locate the position of the stopped kaons and detect the μ^+ from the $K_{\mu 2}$ decay for event identification.

ν_μ decay is 1 sr. The photomultiplier base system has been described elsewhere.⁷

D. Spark-Chamber Detectors

Pion Beam and Kaon-Telescope Triggering Systems

The spark-chamber arrays are also shown in Figs. 3 and 4. Four "foil" spark chambers were used in the pion beam as a part of the momentum spectrometer to measure the momentum of each pion associated with every analyzed kaon event ($X\pi 1$, $X\pi 2$, $X\pi 3$, and $X\pi 4$). Two were upstream and two were downstream of the bending magnet. The last two chambers were also used as part of the π - K system to determine the pion-kaon angle.

There were four spark chambers in the K telescope ($K1$, $K2$, $K3$, and $K4$). The first chamber, a foil chamber, established direction of the kaon from the

⁷ H. F. Davis and H. Spore, IEEE Trans. Nucl. Sci. 12, 245 (1965).

liquid target as accurately as possible without compromising the available acceptance solid angle of the telescope. The second spark chamber, also a foil spark chamber, established the intermediate direction of the kaon. The third and fourth spark chambers were composed of nine plates of $\sim 1/8$ -in. stainless steel, for the stopping-decay regions, with one pair of foil gaps upstream and one pair of gaps downstream from the main body. In these chambers the kaon was observed to stop and decay. The range (energy) of the kaon was determined by the kaon's path and where it stopped in the K telescope.⁸

The π -spectrometer spark chambers were projected on a 35-mm film format through a 105-mm Schneider lens, a prismatic adder, and one mirror for each of the ($X\pi 1$, $X\pi 2$) and ($X\pi 3$, $X\pi 4$) pairs. The elevation views of these spark chambers, though little used, were taken through a $\sim 45^\circ$ mirror. A horizontal stretched string ≤ 1 mm diam was seen in the ($X\pi 1$, $X\pi 2$) view and in

⁸ G. Igo *et al.*, Phys. Rev. 109, 2133 (1958).

the ($X\pi 3, X\pi 4$) view. This gave a consistency check on the optics of the system to minimize optical distortions, and so any accidental variations in the positioning of the optical system would not compromise the data. A similar pair of stretched strings from the ($X\pi 3, X\pi 4$) view to the K -telescope view determined the π - K real-space angle.

The K -telescope spark chambers were projected on another 35-mm film format through a 210-mm Schneider lens with a 30×40-in. mirror mounted 20 ft above the apparatus. The elevation views of these spark chambers were seen through a pair of mirrors mounted on a common aluminum jig plate at $\sim 45^\circ$ to the vertical. Another pair of stretched strings, put in a V shape with the $3^\circ V$ in the horizontal plane, were viewed in the elevation and plane views of the K -telescope format. The plane view of all the spark-chamber tracks was affected by slightly tilting all the spark chambers so the virtual camera was looking approximately parallel to the plates. This caused only a small part of the elevation view of the spark-chamber volume to be "dead."

Several fiducial points were used in both camera formats. The spark chambers were given a general field illumination for each event with flash lamps. The film records were correlated with common sets of Nixie-lamp numbers.

The physical and electrical properties of these chambers are summarized in Table II. In the decay regions K_I and K_{II} , the range spark chambers $K3$ and $K4$ comprised essentially all of the useful volume for the stopping and decay of the K mesons. In all cases

the scintillation detectors limited the production solid angle. The Čerenkov detectors limited the decay solid angle.

It was essential that the two-track efficiency for the range chambers be high for the upstream decay of the $K_{\mu 2}$ muon. On a qualitative basis, assuming all other conditions of scanning are first applied, the heavily ionizing stopping kaon is usually responsible for a much darker track than the near-minimum-ionizing muon.

E. Electronics

There were three classes of electronics used in this experiment: (1) slow logic associated with controlling the experiment in phase with the accelerator; (2) fast logic for AND, NAND logic with scintillation and Čerenkov detectors; and (3) auxiliary systems for driving the spark chambers and all of the devices associated with spark chambers.

The electronics contributed directly to the recorded data in three ways. The electronic scaler counters, recording the number of charged particles into the K telescope, printed out, typically, after 80×10^6 pions on the liquid target (see Table IV, below). Selected scintillation and Čerenkov detector pulsers were displayed on a 35-mm film record of the four-beam oscilloscope trace and had their signals timed-in and gated with low-level logic circuits. The spark-chamber pictures of the pion and kaon events also had recorded on them the light coding of the counters associated with "yes" trigger for the spark chambers. The electronic control logic is shown in Fig. 5. The fast triggering logic is shown in Fig. 6.

TABLE II. K -telescope detector. (a) Scintillation and Čerenkov detectors and (b) spark chambers.

(a) Scintillation and Čerenkov detectors				
Name	Thickness to kaon direction (in.)	(Ref. 8) (g/cm ²)	Principal logical function	Comment
C1	2.8	~ 13	K -NO	FC75 ($n = 1.28$)
S1	0.5	~ 1.3	K -YES	NE102
S2	0.5	~ 1.3	K -NO	NE102
C2	2	~ 6	μ -YES	GLYCOL ($n = 1.47$)
C3	2	~ 6	μ -YES	NE102
S4	0.5	~ 1.3	μ -YES	NE102
C4	2	~ 6	μ -YES	GLYCOL ($n = 1.47$)
S4	0.5	1.3	K -NO	NE102
C5	2	~ 6	μ -YES	GLYCOL ($n = 1.47$)
S3'	0.5	1.3	K -NO	NE102
C6	2	~ 6	μ -YES	GLYCOL ($n = 1.47$)
S4'	2.0	5.1	K -NO	NE102
(b) "Foil" and range-stopping spark chambers.				
Name	Thickness to kaon direction (in.)	[$\frac{1}{4}$ -in. gaps and Ne/He (0.95/0.05) gas] (g/cm ²)	Function	
K1	0.013 Al	~ 0.035 (10-gap)	K^+ direction	
K2	0.009 Al	~ 0.024 (6-gap)	K^+ direction	
K3	0.006 Al; $\frac{1}{8}$ -steel	0.016 (4-gap); 21.2 (8-gap)	K^+ stopping μ^+ track	
K4	0.006 Al; $\frac{1}{8}$ -steel	0.016 (4-gap); 21.2 (8-gap)	K^+ stopping μ^+ track	

Master Control System

The master control system integrated the operation of the experiment. The whole electronic system was tied together through the fast gating of the triggering logic of the π and K electronics and through synchronization with the accelerator beam pulsing of the pulsers for spark chambers, camera advance, Nixie lamps, fiducial lamps, oscilloscope triggering, and the off gating of triggering logic electronics for each kaon trigger signal.

The schematic of the system control logic is illustrated in Fig. 5. The logical operations that the system controlled for the proper synchronization of the experiment are summarized in Table III.

The principal operation of the master control system was finally effected through 0–5-V signals on 50- Ω lines from a gated trigger generator. One complete cycle of the experiment began with the fiducial flash for general field illumination during the beam pulses. The accelerator prepulse gated on the fast logic. The fast logic generated a kaon trigger on getting the coincidence between a pion and kaon signal. The system control initiated a trigger pulse to the spark chambers

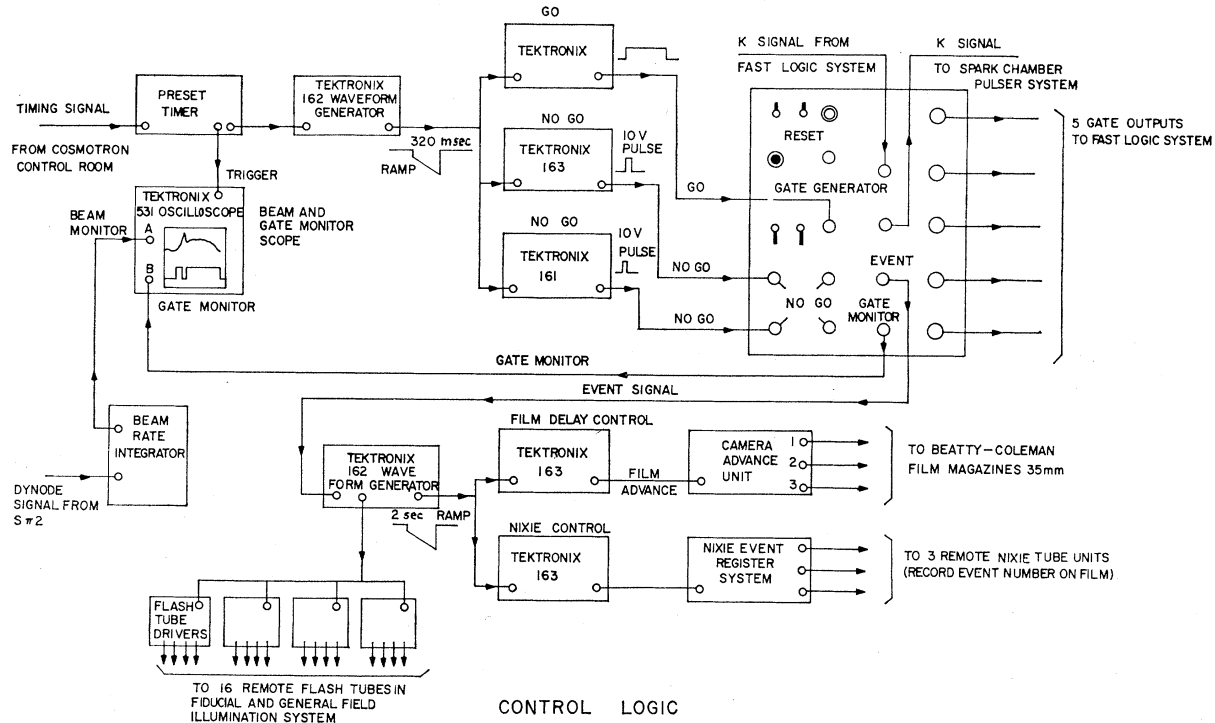


FIG. 5. Control logic. The control logic was a "slow-fast" type of electronic control. It controlled the cycling of events with the 5-sec interval between accelerator beam pulsing, and it controlled the fast, 0.1- μ sec "blanking" of the fast logic after an event was registered during a 0.3-sec beam pulse period.

and simultaneously gated off the triggering logic electronics. The triggering logic gated off until the next beam pulse. The Nixie numbers and general field-illumination lamps were flashed and then the pion and kaon linear gate cameras were advanced. This completed one event cycle. The system control then waited for the next accelerator prepulse to gate on the triggering logic.

Pion Beam Triggering Logic

The pion beam counters π_1 , π_2 , π_3 , π_4 , and π_5 produced anode pulses on 50- Ω lines with $0.5 \leq V \leq 1.2$ V. Tunnel diode discriminators were synchronized to form the coincident blocks $\pi_1\pi_2$, $\pi_3\pi_4$, $\pi_1\pi_2\pi_3\pi_4$, and $\pi = \pi_1\pi_2\pi_3\pi_4\pi_5$. The resolving time in the yes twofold blocks was ~ 3 nsec. The "no" resolving time was ~ 7 nsec. The typical ratio of counts in these four channels was $\sim 3:2:1:1$. There was a significant singles rate in the π_1 and π_2 counters apparently due to low-energy phenomena; this was about three times the $\pi_1\pi_2$ rate. The $\pi_1\pi_2\pi_5$ rate was about equal to the $\pi_3\pi_4$ rate.

There were too few "true" double pulses in the pion beam to justify an electronic guard that would have discriminated against beam events that came within the spark-chamber memory time without unnecessarily limiting the amount of data collected; these events were later discarded. With $\sim 10^5$ pions per pulse with a spill of 0.3 sec, the average separation was ~ 3 μ sec. Although

there was no apparent rf structure on the beam pulse, there were periodic intervals during the beam spill which corresponded to "spikes" on the singles rate of the beam counters; this potentially bad effect was suppressed by simply gating off the fast logic during these periodic intervals.

It was established through checks that consistently

TABLE III. The master control. (a) Logical functions; (b) pulsing system.

(a) Logical functions	
(1)	Gated on fast logic during accelerator pulse
(2)	Gated off fast logic during high-duty periods
(3)	Gated off fast logic after a kaon event
(4)	Gated on camera advance
(5)	Gated on fiducial flash lamps
(6)	Gated on light coding element
(7)	Gated on four-beam scope
(8)	Gated event number registration advance
(9)	Gated on spark-chamber pulser
(b) Pulsers	
Pulse drivers for	
(1)	Camera advance
(2)	Fiducial flash lamps
(3)	Light coding elements
(4)	Event number registration
(5)	Spark-chamber pulsing

FAST TRIGGERING LOGIC

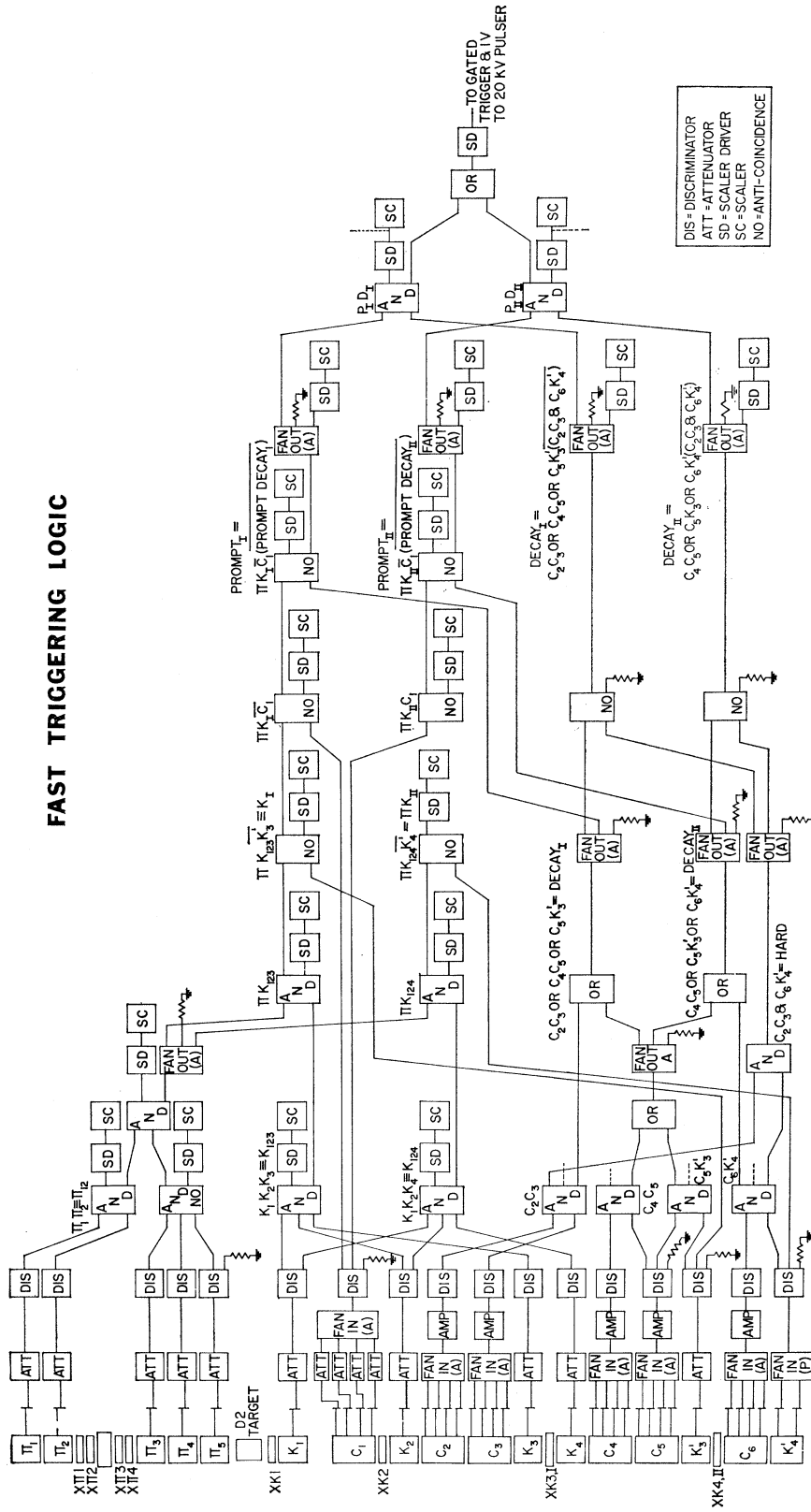


Fig. 6. Fast triggering logic. The fast electronics were divided between the pion beam and the kaon systems. The kaon system was divided into the kaon "prompt" part (in prompt coincidence with the pion system) and the muon "delayed" part (in coincidence with the delayed signal from the "prompt" part).

95% of the particles that passed through our momentum spectrometer and were incident on the liquid flask were counted; if there had been fluctuations in this rate, they could have caused a significant change in the background and an unnecessary number of false triggers.

The π events were registered on the scaler counters and were used to form a coincidence between various logic blocks in the kaon triggering logic.

Kaon-Telescope Triggering Logic

The fast-logic block diagram for kaon telescope triggering is shown schematically in Fig. 6. There were three "stopping" and "decay" regions of the K telescope that could initiate a trigger for the pulsers of the spark chambers.

The kaon triggering signal which caused the spark chambers to register an event in region K_1 was associated with the following logic condition: $(S_1S_2S_3\bar{S}_4C_1)$ AND $(C_2C_3$ OR C_4C_5 OR $C_5C_3')$. The $(S_1S_2S_3\bar{S}_4C_1)$ corresponded to a charged particle that came into the telescope and stopped but with a speed too small to trigger C_1 . Secondly, the delayed coincidence between this prompt block and any of the three decay channels corresponds to a decay event from the stopped particle. The yes coincidence resolving times were typically 4 nsec while the no resolving time was about 8 nsec. The delayed coincidence time was, typically, 6–8 nsec after the prompt event and extending for 20–28 nsec.

Similarly, the kaon triggering initiated the spark chambers for the registration of a K_i event for the logic condition $(S_1S_2S_4\bar{S}_3\bar{C}_1)$ and $(C_4C_5$ OR $C_5S_3')$.

As specifically as this triggering was designed to see only kaons and not pions and protons, it finally gave a (signal/background) $\sim 1/75$. This kaon detector was looking for short-lived kaons from an effective cross section into our telescope of $\lesssim 20 \mu\text{b}$; the total πd cross section is $\sim 50 \text{ mb}$.

Auxiliary Electronic Systems

1. Light coding system. The light coding was a set of lights, mounted on top of the counters C_4 and C_5 in the K telescope, that were illuminated if certain fast-logic coincidences were satisfied. Logic signals were gated, with an ~ 75 nsec coincidence resolving time, with a kaon trigger pulse from the fast-logic system.

The light coding, recorded on the spark-chamber film, gave a visual check between the fast-logic coincidences and the tracks of the event as they appeared in the spark chambers of the kaon telescope. It proved an invaluable part of the data. Although many of the false triggers were obvious without consulting the light coding, parts of the data were recovered by demanding that the light-coding data not be inconsistent with the event as it appeared in the spark chambers.

The light coding system was positioned physically

next to the spark chambers. Though it was very susceptible to pickup from the spark-chamber pulsing, it was established, after considerable design and testing, that the light-coding data were not influenced by the spark-chamber pulsing.

2. Spark-chamber pulsing system. The spark-chamber pulsing system was comprised of a pulser: (1) input pulse $\gtrsim 1$ V, 30 nsec on 50- Ω line; (2) output pulse $\gtrsim 22$ kV, 40 nsec, on a 50- Ω line with a delay time $\lesssim 45$ nsec. The rest of the system was composed of voltage fanouts, using four and six output slave gaps, followed by a series of current fanouts, using 1:4 pulse transformers of 50 Ω in an 50 Ω out, to bring the voltage down to ~ 8.5 kV pulses to the individual gaps of the spark chambers.

The gaps of the spark chambers were driven with charged capacitors and transmission lines in such a way as to suppress the gap-to-gap robbing. This system is illustrated in Fig. 7. The discharge of one gap of a spark chamber, causing a low-impedance load, was not seen by any of the neighboring gaps until ≥ 25 nsec later, owing to the ~ 13 -nsec cable from the transformer to the spark gap. The ferrite core next to the spark chamber further increased the instantaneous gap-to-gap impedance by presenting a high-impedance path to reflected pulses between cable sheath and "world ground." Spark chamber K_1 was checked for gap-to-gap robbing for over 10 000 minimum-ionizing tracks; fewer than five could be interpreted as gap-to-gap robbing.

3. Linear gate system. The outputs from a selected number of counters were displayed in prefixed time ones on a four-beam oscilloscope after passing through a linear gate system, a system which was gated on by the action of a positive kaon-trigger from a kaon-telescope- π -beam coincidence.

The dynode signals were synchronized with the fast-logic electronics for gating. There were, typically, four series of pulse on each of the four oscilloscope traces. The gating signals were set to open gates for ~ 45 nsec. The gating pulse was adjusted to the most sensitive signal pulse response, leading to a pedestal of about 50 mV if no signal pulse was seen. The dynamic response of the system was about 25 mV to 2 V; it was only approximately linear. There was less than 10 mV feed-through for a normally off gate with a ~ 2 V input.

This system served several functions. Its operation early in the data taking ensured that the scintillation and Čerenkov counters responsible for the triggering were functioning as indicated by the fast-logic circuits. Its checked performance as measured throughout the data taking ensured the continued reliable performance of the counter and fast-logic systems. It was used to check the K events as obtained from the scanning. The kaon events must not be associated with a pulse from C_1 , the liquid Čerenkov counter with a velocity threshold higher than the positive kaon stopping in the kaon telescope. The pulse discrimination level from C_1

could not be lowered too much below 250 mV without increasing the antidead time; thus with the linear gate sensing pulses down to ≈ 50 mV it was also a backup anticoincidence element.

III. DATA

The data collected on the deuterium-target running, reaction (1), and from the hydrogen-target running, reaction (2), are the principal "running" data. Other data were comprised of the surveys of the spark-chamber fiducial system and the momentum-spectrometer-magnet calibration.

There are few significant differences between the deuterium- and the hydrogen-target running conditions. In fact, the hydrogen-target runs were designed to be as similar as possible to the deuterium-target run to make the calibration as true as possible. The same physical target was used in both runs; liquid hydrogen rather than liquid deuterium was used to fill the target's primary inner flask for the calibration running. The same triggering system, detectors, and electronics were used for both kinds of runs; the same spark-chamber

system was used for both kinds of runs. However, because the same range spark chambers, for stopping the produced positive kaons, were used, the kinematics of reaction (2) demanded that the mean beam momentum be increased from ~ 1.15 GeV/c to ~ 1.4 GeV/c. The two-body kinematics for $\pi^- + d \rightarrow K^+ + (\Sigma^- n)$, (1), and for $\pi^- p \rightarrow K^+ + \Sigma^-$, (2), differ in a substantive way for the range of sensitivity of the common kaon detector. The value of

$$\left. \frac{\partial T_{K^+ \text{lab}}}{\partial \theta_{K^+ \text{lab}}} \right|_{T_{K^+ \text{lab}}=250 \text{ MeV}, \theta_{K^+ \text{lab}}=45^\circ}$$

is 6.7 MeV/deg for Σ^- production from the hydrogen target, $P_{\pi \text{lab}} = 1.4$ GeV/c, and 3.3 MeV/deg for assumed $(\Sigma^- n)$ production from the deuterium target, $P_{\pi \text{lab}} = 1.15$ GeV/c. Thus, the common kaon detector had a higher sensitivity for the set of kaons from the assumed $(\Sigma^- n)$ reaction than from the Σ^- reaction. The kaon yield for reaction (2) was much less than the kaon yield from reaction (1) (see Fig. 8). The calibration data led to results on the detector system's mass scale,

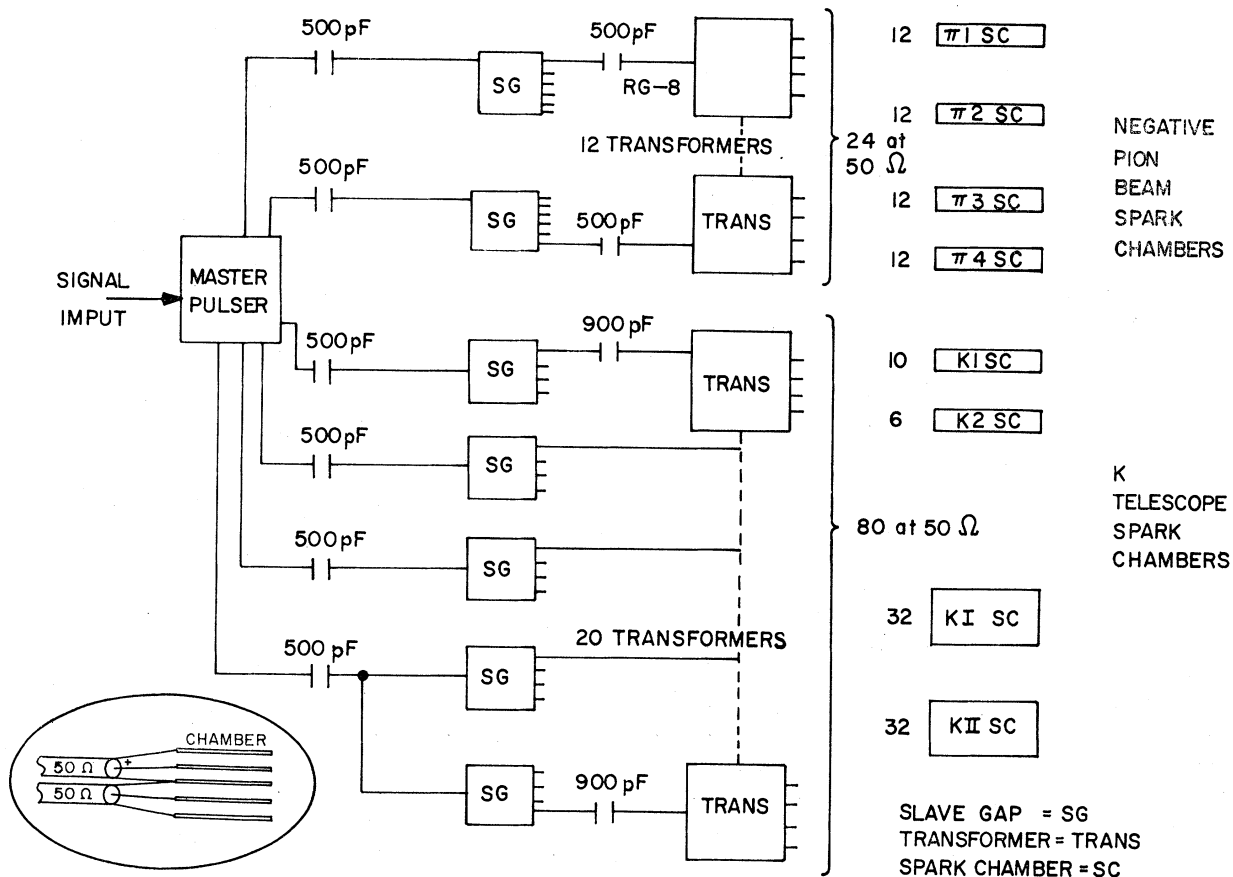


FIG. 7. The spark-chamber pulsing system was principally a 1 V-to-20 kV 50-nsec-delay pulse generator driving voltage fanouts which in turn drove 1:4 pulse transformers. All of the plates of the spark chambers were driven with charged transmission with 50-, 25-, or 12.5- Ω impedances. The manner of coupling the transmission lines to the plates of the spark chambers virtually eliminated gap-to-gap pulse robbing.

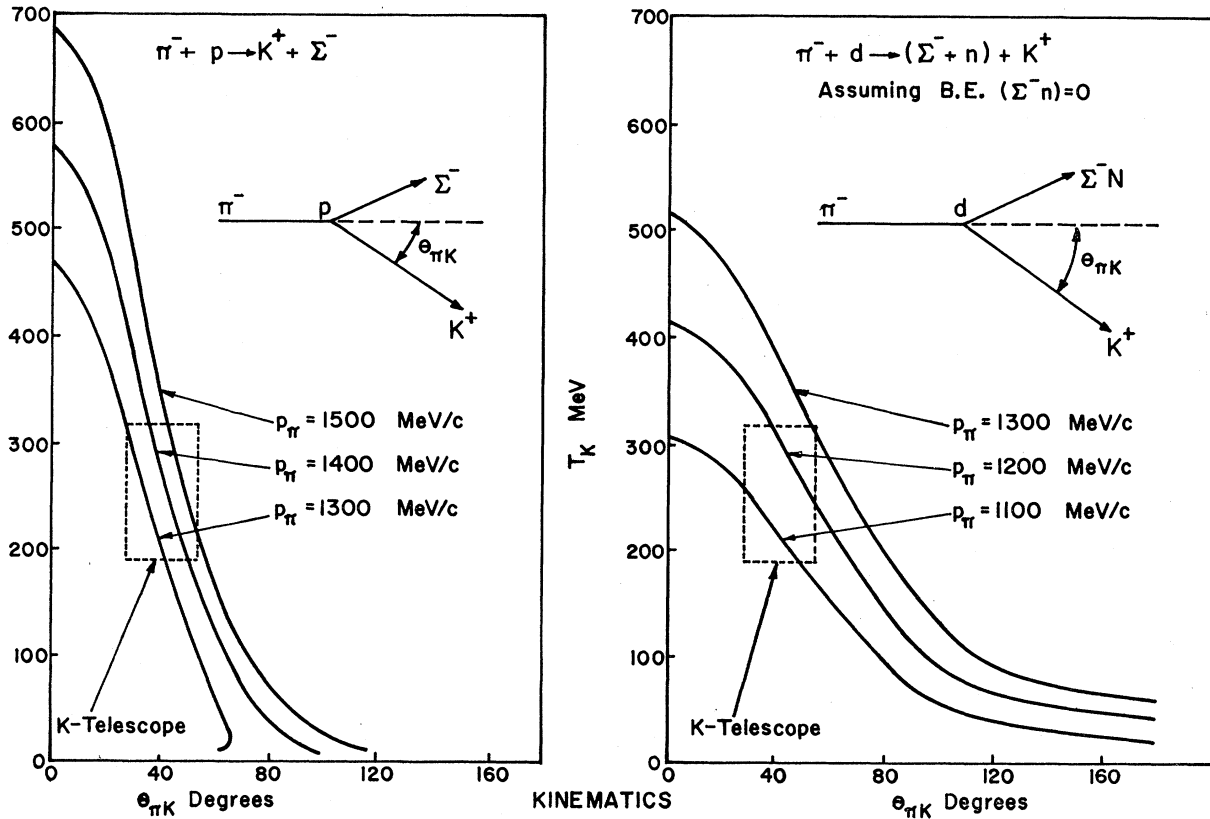


FIG. 8. This shows the kinematics in the laboratory frame for the two reactions: $\pi^- + p \rightarrow K^+ + \Sigma^-$ at 1.4 GeV/c and $\pi^- + d \rightarrow K^+ + \Sigma^- + n$ at 1.15 GeV/c. In addition, the region of acceptance of the kaon telescope is traced out to show the kinematics of the kaon telescope.

the Σ^- mass, but could not, because of this, be used for a cross-section measurement of reaction (2).

The following subsections are basically a summary of these raw data: (1) the film data from the pion momentum spectrometer and the kaon telescope, and the counting "running" data; (2) the basic parts of the survey and momentum-spectrometer-magnet data.

A. Data Acquisition

The primary data were taken over a four-week period. The experiment was set up and taken through a preliminary test period during a prior four-month period.

The systematics of the primary-data acquisition centered on run through of check procedures that gave credence to the quality of performance of the system. The running data that were most readily checked were those from the scaler counters that registered the performance of the individual detectors and fast-logic elements. The "format" of the scaler counters is illustrated in Table IV. The running was divided into runs of preset count of typically 80×10^6 pions incident on the flask of the liquid target. Taking no more than one spark-chamber data trigger per beam pulse, there was then a running check on the counter-electronic

performance as well as a monitor of the number of pions on the liquid target. About 170 h were devoted to tuning the pion transport system and setting up and measuring the characteristics of our pion momentum spectrometer. About 225 h were used strictly data taking. An additional 25 h were used for "routine" checks.

B. Hydrogen-Target Data

The data taken from the calibration reaction $\pi^- + p \rightarrow K^+ + \Sigma^-$ are comprised of approximately 7800 pictures. The sensitivity of the kaon detector system to this reaction channel is illustrated in Fig. 9.

C. Deuterium-Target Data

The data taken from the principle reaction $\pi^- + d \rightarrow K^+ + \Sigma^- + n$ are comprised of approximately 70 000 pictures. The sensitivity of the kaon detector system to this reaction channel is also illustrated in Fig. 8. The kaons detected had kinetic energies in the range $190 \lesssim KE \lesssim 320$ MeV in the angular range of $25^\circ \leq \theta_{K\text{lab}} \lesssim 60^\circ$. Table V also summarizes the deuterium-target data.

D. Auxiliary Data

Auxiliary data in this experiment were the survey of the optical system comprised of the flat mirrors,

TABLE IV. Triggering rates in the different elements of the (a) pion and (b) kaon detector systems.

		(a) Pion beam logic	
Name	Logical unit	Flux	
Pion beam	$\pi = \pi_1 \pi_2 \pi_3 \pi_4$	75 000 to 150 000 per 0.3 sec beam pulse	
"Shadow" pion beam	$\pi_1 \pi_2 \pi_5$	~50 000 per beam pulse	
(b) Kaon-telescope logic			
Name	Logical form	Function	Number
π	$(\pi_1 \text{ AND } \pi_2) \text{ AND } (\pi_3 \text{ AND } \pi_4) \text{ NAND } (\pi_5)$	π beam	10^6
K_{123}	$S_1 \text{ AND } S_2 \text{ AND } S_3$	Charged particle into K telescope	3×10^3
K_{124}	$S_1 \text{ AND } S_2 \text{ AND } S_4$		2.2×10^3
πK_{123}	$\pi \text{ AND } K_{123}$	π -induced charged particle	1.2×10^3
π_{124}	$\pi \text{ AND } K_{123}$		850
πK_I	$(\pi K_{123}) \text{ NAND } (K_3')$	Stopping-pion-induced charged particle	580
πK_{II}	$(\pi K_{124}) \text{ NAND } (K_4')$		501
Decay _I	$C_2 C_3 \text{ OR } C_4 C_5 \text{ OR } C_5 S_3'$	Minimum-ionizing particle	71×10^3
Decay _{II}	$C_4 C_5 \text{ OR } C_3 S_3' \text{ OR } C_6 S_4'$	Minimum-ionizing particle	37×10^3
$\pi K_I \bar{C}_1$	$(\pi K_I) \text{ NAND } (C_1)$	Low-speed stopping-pion-induced charged particles	229
$\pi K_{II} \bar{C}_1$	$(\pi K_{II}) \text{ NAND } (C_1)$		
$P_I D_I$	$(\pi K_I \bar{C}_1) \text{ delayed AND } (\text{Decay}_I)$	Low-speed stopping-pion-induced charged particle in delayed coincidence with minimum particle	61
$P_{II} D_{II}$	$(\pi K_{II} \bar{C}_1) \text{ delayed AND } (\text{Decay}_{II})$		37

the stretched strings, the fiducial markings, and the spark-chamber positions. The survey was done with a spatial accuracy of ~ 0.2 mm. The "hot-wire" method was used to calibrate the spectrometer bending magnet to determine the absolute momentum of the pion beam on an event-by-event basis. The measurement of the bending magnet $\int B \cdot dl$ was done within an error of $\sim 0.2\%$; this was not the limiting error in the momentum measurement. There were also scaler counting data. The most significant factor from this is the measured (target empty)/(target full) ratio. The π -K kaon events of the electronic logic of Fig. 6 had a (target empty)/(target full) ratio of $< 1/60$.

IV. DATA REDUCTION

The data reduction involved (1) calculations establishing the spark-chamber fiducial system's true spatial positions; (2) calculations establishing the momentum spectrometer's true calibration from the data from the measured magnet properties; (3) scanning and the measuring of the film-data events; (4) final editing, spatial reconstructions, and the kinematical calculations which combined the results of the first three parts to give the sample of events of reaction (1) and a sample of events of reaction (2); (5) the detector counting data are combined with part (4) to give a raw data $M(\Sigma^-n)$

TABLE V. Summary of data runs.

Pion beam momentum (GeV/c)	Target	No. events
1.08*	Deuterium	20 000 pic.
1.20*	Deuterium	45 000 pic.
1.4	Hydrogen	4000 pic.
1.25	Hydrogen	3800 pic.

* Average for all deuterium data 1.15 GeV/c.

distribution for the sample of events from the deuterium data; (6) finally, the detector system's absolute detection efficiency as a function of beam momentum, kaon energy, and angle is calculated to obtain the differential cross section $d\sigma/dM(\Sigma^-n)$ in the range from $\sim M_0(\Sigma^-n) - 100$ MeV to $\sim M_0(\Sigma^-n) + 150$ MeV.

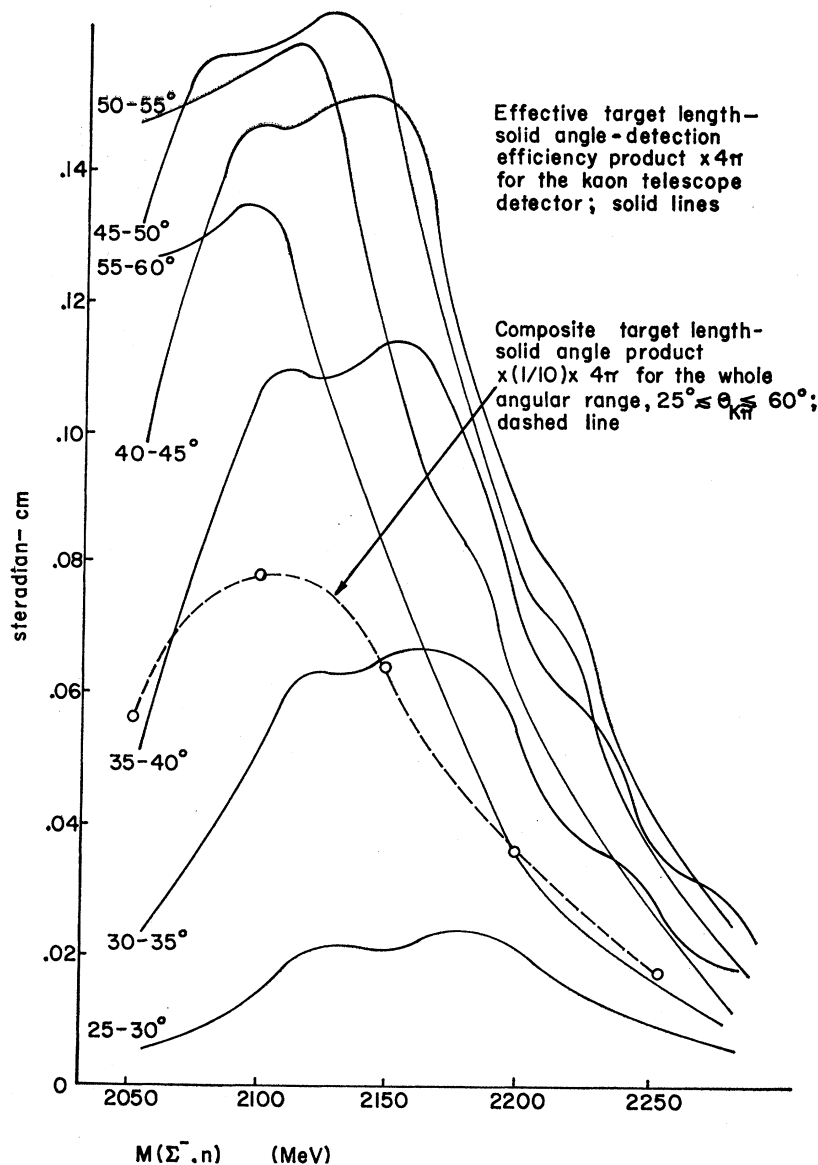
A. Auxiliary Data

The auxiliary data were comprised of the survey of the fiducial system and the hot wire calibration of the pion-momentum-spectrometer bending magnet.

The optical system was composed of flat-plate spark chambers, flat mirrors, and fiducial points. There were two optical systems. The kaon detector was composed of four spark chambers, a pair of stretched strings, fiducial markings, two side mirrors, one large (30×40 in.) over-all mirror, and a 210-mm Compenon lens focusing the 30×60-in. image onto a 35-mm format (see Fig. 10). The pion detector was composed of four spark chambers, several stretched strings, four side mirrors, fiducial marks, and a small flat-mirror configuration in front of a 105-mm lens to overlay the images of the two pairs of sharp chambers. The stretched strings tied the data from the two camera systems together.

The result of spark-chamber displacements on the accuracy of the data is less than second order because of the small effect on the data on the absolute position of the chamber plates. The mirrors were supported on three points on a 1-in. Al jig plate. The optical distortions due to possible mirror curvature were negligible even for the large (30×40 in.) overhead mirror. The fiducial markings were surveyed to $\lesssim 0.2$ mm in laboratory space. The stretched string, although moved several times, was straight to within a fraction of its width, 1 mm, over its several-meter length. The lens

FIG. 9. Calculated detector efficiency as a function of (Σ^-n) invariant mass averaged over the different beam pion momenta. It has folded into it the effect of location of kaon production in the target, the $K-\pi$ angle and kaon energy. It is primarily a geometrical efficiency factor. Its units are cm sr.



systems produced no optical problems that could not be handled by pin-hole approximations.

The useful aperture of the 18×36 -in. bending magnet used in the momentum spectrometer was calibrated with a hot-wire instrument. The integral $\int \mathbf{B} \cdot d\mathbf{l}$ over the useful aperture was $\leq 0.2\%$. As a check, this was done on another identical magnet of the same class, and the same result was obtained. That this absolute calibration was effective is seen from the measurement of the Σ^- mass, 1199 ± 6 MeV.

B. Film Scanning and Measuring

The total 77 800 frames of film were scanned three times. The detection efficiency for scanning for positive kaon decay was (first scan missed but seen by second scan)/(first scan) = 0.95. After the kaon-telescope event

was identified the pion event was examined. A significant fraction of the data was compromised in the pion system owing to spurious tracks and to a lesser extent to intermittent efficiency of the last pion spark chamber. It was necessary to have only one clear track in all of the pion spark chambers to be able to make unique reconstruction of the events. The kaon events were classified according to where the kaon stopping in the range chamber system and according to upstream or downstream μ from $K_{\mu 2}$ decay. Only the upstream $K_{\mu 2}$ events were used in the deuterium data. The upstream $K_{\mu 2}$ events from the deuterium data gave a somewhat better signal-to-background ratio in determining the (Σ^-n) invariant mass. The downstream events were more susceptible to contamination from scattering than the upstream events. The efficiency of the kaon detector

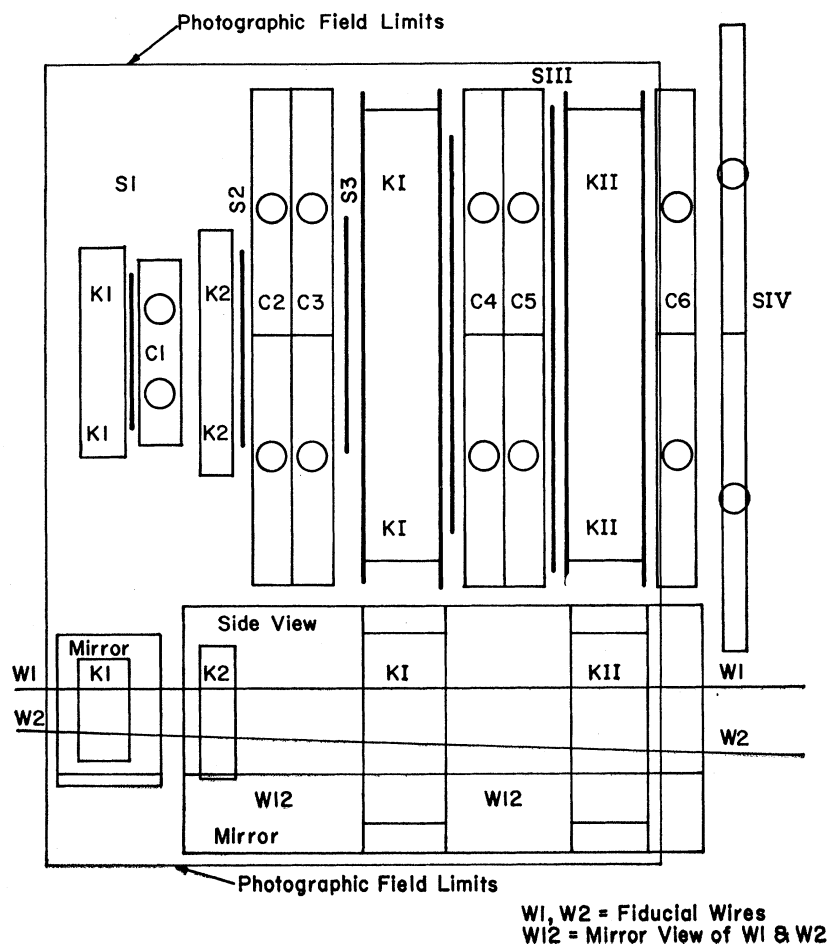


FIG. 10. Data format of the views of the spark chambers.

K TELESCOPE AREA - TOP VIEW

system was calculated in order to correct for the loss of the downstream events.

The film measuring was done with a measuring machine described previously.⁹ Basically the machine had an $\sim 15:1$ magnification. The digitization of the data was through a 3600 bit 360° angular encoder mounted on a drafting arm. This image-plane machine digitized the data in 0.1° bits over approximately a 24×30 -in. image region. The resultant effective spatial digitization bin on the ~ 20 -in. lever arm was dependent on the position of the data in the fiducial volume and

was generally no more than 0.07 in. in the image-plane space. This produced an error of 0.6 mm in laboratory space. This was the limiting error in the pion momentum measurement. The kaon range (energy) measurement was not limited by this. However, the pion-kaon angle measurement was nearly equally limited by this and the natural spark-chamber track spread.

At least three points were measured in all of the spark-chamber tracks. All of the upstream events were measured twice. The efficiency for events passing the measuring requirements was about 0.99.

After all of the events had been scanned and measured, the events which had passed were then re-examined by the physicists. A small fraction of the data still had in it events which satisfied looser criteria than expected from the application of the original scanning criteria. Specifically, kaon-decay events had been kept when it was clear that the so-called μ track from the so-called kaon track did not meet, but in fact crossed. The elimination of these ~ 11 "events" from the data removed events from a wide range of $M(\Sigma^-n)$, both

TABLE VI. Summary of data reduction.

	Hydrogen data	Deuterium data
Number of events	~ 7800	$\sim 70\,000$
Number of scanned events	~ 200	$\sim 1\,300$
Number of one-pion-track events	~ 90	~ 270
Number of $K_{\mu 2}$ upstream μ -decay	43	211

⁹ H. F. Davis *et al.*, Phys. Rev. **131**, 2192 (1963).

TABLE VII. Range of values and errors of directly measured quantities.

Name	Range of values	Error	Method
$B \cdot dl$	12 000 to 14 000 kGm	$\sim 0.3\%$	Hot-wire method
$\pi 1, \pi 2, \pi 3, \pi 4$ π^- -track directions	mean $+5^\circ$ to mean -5°	± 0.001 rad	Spark track fitting
$K1, K2$ K^+ -track direction } Kaon stopping point	$45^\circ + 15^\circ$ to $45^\circ - 20^\circ$ ~ 40 to 88 g/cm ² of carbon equivalent (Ref. 8)	± 0.005 rad $\pm \frac{1}{16}$ in. of steel	Spark track fitting Spark track

below the above M_0 . The application of successive measurements of single tracks which were "straight-throughs" leads us to the determination of the natural track spread of $\lesssim 0.3$ mm in the spark chamber in laboratory space.

The results of the scanning and measuring are summarized in Table VI. There were 1020 stopped kaon events from the 70 000 deuterium pictures. Approximately half of these were eliminated because only upstream events were kept. The cross section was corrected for the exclusion of both the "downstream" events and events with multiple pion tracks. These two factors are folded into the kaon-telescope detection efficiency to give the results of Fig. 9.

C. Editing, Spatial Reconstruction, and Kinematical Fitting

The data were measured event by event and recorded in fixed format on IBM cards. Events which failed simple criteria were remeasured or upon further examination were discarded. The next stage was the fitting of straight lines to all of the measured spark-chamber tracks. This geometrical reconstruction of particle trajectories in laboratory space gave three lines; the upstream and downstream beam pion trajectories, and the kaon trajectory. These were then used to calculate θ_π (the angle of deflection of the beam pion through the spectrometer magnet), $\theta_{K\pi}$ (the angle between the beam pion and the produced kaon), and the kaon path through the kaon telescope. The error matrices on the individual events were calculated. The approximate position inside the liquid target from which the event originated and the beam pion momentum were calculated. The range of values of these different parameters and the errors associated with them are given in Table VII.^{9a}

D. Uncorrected (Σ^-n) and Σ^- Mass Distributions

The reduction of the hydrogen-target data gave a set of events for which the following was known: θ_π , $\theta_{K\pi}$, range of the kaon, and the fact that the event actually occurred in the body of the liquid hydrogen. These data were used to determine $p_{\pi\text{lab}}$, and $\text{KE}_{K\text{lab}}$. Along with $\theta_{K\pi}$, these were used to calculate the invariant

^{9a} The recent range (energy) tables used in determining the kaon range (energy) T_K were compiled by W. Barkus and M. Berger, Nat. Acad. Sci. 1133 (1965).

mass of the Σ^- hyperon. The invariant mass distribution is shown in Fig. 11. The measured mass $M_{\Sigma^-} = 1199 \pm 6$ MeV establishes two points: The kaon detector system is really a kaon detector, and the absolute calibration of the kaon range (energy) and the pion momentum are true. Only events from upstream μ 's from $K_{\mu 2}$ decay are incorporated in these data.

The results from the deuterium-target data are also shown in Fig. 11. These are the raw data. This is the number distribution of events $M(\Sigma^-n)$ which passed the scanning criteria. The detector system's efficiency factors are not incorporated into this. An error analysis gives a $M(\Sigma^-n)$ resolution (half-width at half-maximum) of 8 MeV. Of course this is different from the Σ^- -mass resolution because of kinematical factors. The most significant factor about this $M(\Sigma^-n)$ distribution is the near total absence of events for

$$M(\Sigma^-n) \lesssim M_0(\Sigma^-n) = 2137 \text{ MeV.}$$

In fact, the number of events for $M(\Sigma^-n) \lesssim M_0(\Sigma^-n)$ in the deuterium data is consistent with the background level in the hydrogen-target data for events in Σ^- -mass distribution for non- Σ^- -mass.

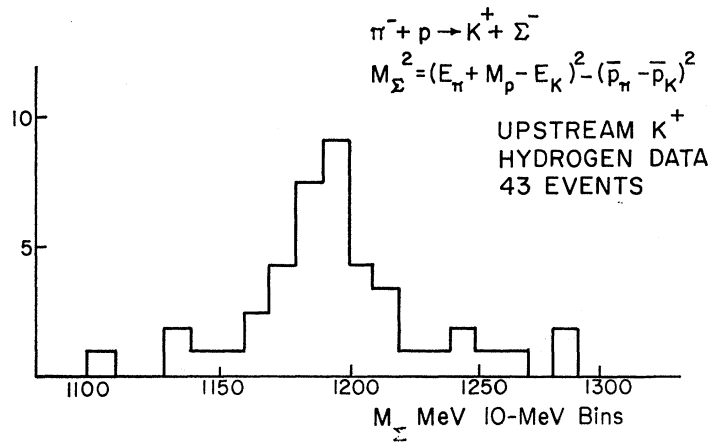
The momentum p_π , the kinetic energy KE_K , the angle $\theta_{K\pi}$, and the $M(\Sigma^-n)$ values and errors were summarized in Table VIII. It is important to note that the measured Σ^- -mass resolution of the detector system was essentially that of the calculated resolution based on the propagation of errors on the individual parameters. The range (energy) of the kaons through the different materials of the telescope gave a KE_K resolution (half-width at half-maximum) of 5 MeV. The pion-beam-momentum measurement of 0.5% was the principal factor in the $M(\Sigma^-n)$ resolution.

E. Detection Efficiency

The absolute detection efficiency of the kaon detector was ~ 0.074 sr cm for 1.15-GeV/ c pions and 225-MeV

TABLE VIII. Range of values and errors of determined quantities.

Name	Range of values	Error
Pion momentum P_π	1 to 1.5 GeV/ c	0.7%
Kaon-pion angle $\theta_{K\pi}$	25° to 60°	$\pm 0.3^\circ$
Kaon range-energy ⁸ T_K	190 to 310 MeV	± 5 MeV
(Σ^-n) invariant mass, $M(\Sigma^-n)$	2137-100 to 2137+150 MeV	± 8 MeV



(a)

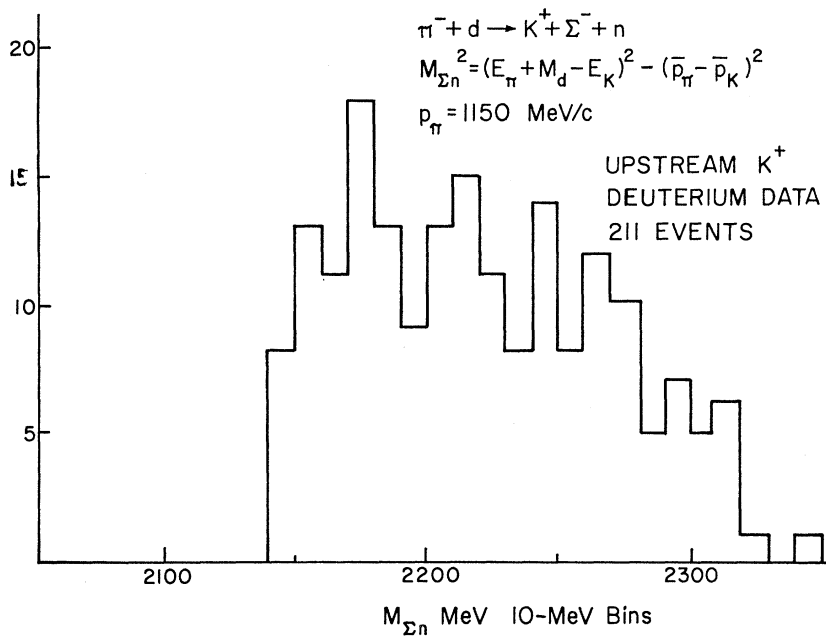


FIG. 11. (a) Number distribution of events as a function of Σ^- invariant mass as measured in the calibration reaction $\pi^- + p \rightarrow K^+ + \Sigma^-$. The mass scale of the system was calibrated from the result that Σ^- invariant mass is $1199 \pm 8 \text{ MeV}$. (b) Number distribution of events as a function of $(\Sigma^- n)$ invariant mass as measured in the reaction $\pi^- + d \rightarrow K^+ + \Sigma^- + n$. These raw data are multiplied by an event-by-event detection efficiency to give the differential cross section.

kaons at $\theta_{K\pi} \cong 45^\circ$. This is the product of several factors: (i) the average kaon telescope (solid angle) (target length), (ii) the probability of the produced 225-MeV kaon not scattering out or decaying before stopping, (iii) the probability that the kaon decays into the $K_{\mu 2}$ channel and produces a detectable muon into the upstream section of the telescope, and (iv) the probability that the kaon decays within the 6–28-nsec electronic gate period after it stops. Other factors proved to be negligible, such as losses due to counter inefficiencies and due to kaon detection by the C_1 Čerenkov detector (which would exclude counts through the veto logic).

Solid-Angle-Target-Length Product

The detector solid angle was $\sim 0.12 \text{ sr}$ as determined by the geometrical shapes of the scintillation detectors

as determined from a point in the center of the liquid-hydrogen target along the center line of the kaon-telescope detector system. The solid angle that the kaon telescope presented to a 225-MeV kaon varied with $\theta_{K\pi}$ and the position of kaon production in the target. The strongest dependence was on the longitudinal position of kaon production in the liquid target (longitudinal with the pion beam). The effective length of the target is 8 in. out of the 20-in. geometrical length.

Scattering Losses

The scattering losses were calculated on the basis of a total kaon-matter cross section mean free path of 175 g cm^{-2} of matter. This correction is typically of the order of 0.86 .³

Kaon Decay in Flight

This is a small correction. It is typically only of the order of 0.75.

Branching Ratios

This branching ratio is taken to be 0.64 from a recent compilation.¹⁰ There is the additional factor that the other kaon decay channels, $K_{\pi 2}$, for example, could, in principle, contribute to the enhancement of the kaon detection efficiency over and above the $K_{\pi 2}$ decay channel. However, the ethylene-glycol-filled Čerenkov detectors used to detect the K progeny were not sensitive to these other channels. There were, however, among the data, events which indicated we probably had a few $K\pi_3$ events in which the π^0 was γ -ray converted and produced electrons which were detected in the glycol-filled Čerenkov detectors.

Muon Detection Efficiency

The probability of detecting the $K_{\mu 2}$ 236-MeV/ c muon was approximately 0.15.

Electronic Time Gate Efficiency

To avoid detecting scattered particles, the “decay” detector signals sensitive to the muon were in coincidence with a signal from the kaon-sensitive scintillators for a 20-nsec period 8 nsec after the generation of the prompt kaon signal. Because of the physical size of the decay Čerenkov detectors, $2 \times 18 \times 18$ in., and the high optical reflectivity on their inside surface, a prompt background signal in them could give a pulse ≥ 20 nsec after the initiating particle actually passed through the detector. This effect reduced the effective discriminating power of the decay Čerenkov detectors for selecting kaon decay over prompt background processes. This was a contributing factor to the approximately one-to-seventy-five kaon-to-background in the film data. This effect could have been suppressed by increasing the discrimination level from the decay Čerenkov detectors; this would have lowered the kaon detection efficiency. The effective efficiency for a kaon being detected within the electronic gate period was approximately 0.47.

Composite Kaon-Telescope Detection Efficiency

The composite detection efficiency for the kaon telescope for the reaction channel $\pi^- + d \rightarrow K^+ + \Sigma^- + n$ is shown in Fig. 9. This is averaged over the pion beam momenta.

The detection efficiency was applied to the data in an event-by-event calculation. This is described in Sec. VI. The approximate composite target-length-kaon-telescope efficiency is ~ 0.029 sr in. This included the effect of cutting out downstream $K_{\mu 2}$ -decay and multiple-pion-track events.

¹⁰ Particle Data Group, Rev. Mod. Phys. **41**, 109 (1969).

V. BACKGROUND

The background effects need to be examined in light of the basic identification criteria of stopped kaons with $K_{\mu 2}$ decay. Reaction (1) is assumed to have occurred if these criteria are satisfied. There are two principal kinds of background. There are events due to kaons not produced in reaction (1) and events from conditions that simply simulate stopping kaons.

The techniques for reducing the two kinds of background to working levels were incorporated in the triggering logic, the film-scanning process, and the event reconstruction process. The system of counter detectors and triggering logic was designed to preferentially select low-energy kaons. The visual scanning of the range-chamber-system film data for the characteristic kaon “tag” of a stopping kaon with an associated track, $K_{\mu 2}$ decay [$K^+ \rightarrow \mu^+ (236 \text{ MeV}/c) + \nu_{\mu}$], proved effective in selecting kaons over background. Background due to kaons not from reaction (1) was suppressed by requiring the reconstructed tracks from the beam pion and produced kaon be consistent with production in the liquid volume of the target system.

The principal characteristics of the triggering logic which were effective in suppressing background and of efficiently detecting reaction (1) are incorporated in the pion beam system and the kaon telescope. The elements of the pion beam system are illustrated in Fig. 3 and summarized in Table I. The elements of the kaon system are illustrated in Fig. 4 and tabulated in Table II. The beam pion did not pass through an annular ring area directly in front of the heavy frame of the vacuum housing of the liquid target because the last YES counters had air light pipes and there was a NO counter of annular ring shape. The counting was virtually free of chance triggers through the use of short coincidence resolving times and a sufficient number of detectors. The particles which “stopped” in the three sections appeared to stop through the use of NO counters downstream from each of the three sections. The events were consistent with $K_{\mu 2}$ decay (they were associated with a stopped particle in delayed coincidence with a penetrating high-speed particle) because large solid-angle highly efficient Čerenkov counters “sandwiching” each section were operated in delayed coincidence with the prompt signal from the scintillation detectors. The (target empty)/(target full) ratio for kaon-triggered events was $< 1/60$. There were $\sim 10^8$ particles entering the kaon-range system for each triggered event. There were approximately (seventy-five-to-one)/(events-to-stopping kaon events) in the film data.

The principal characteristic of the scanning was the visual identification of events in the kaon telescope’s spark chambers consistent with $K_{\mu 2}$ decay. This proved to be a simple and highly effective means of selecting stopped kaons. The latter was effective both in establishing that reaction (2) occurred and in the calibration

of the system's mass scale through the direct measurement of the Σ^- mass (see Fig. 11). Finally, the reconstructed pion beam and kaon particle trajectories to interaction in the liquid-deuterium target's flask eliminated essentially all of the remaining background events due to kaons not from reaction (1).

A. Pion and Proton Background

There were ~ 30 penetrating charged particles incident on the kaon telescope per kaon trigger from the triggering logic. Positive and negative pions and protons were the principal source of background. A pion reaching the range-measuring regions of the kaon telescope had triggered the C_1 -FC75 filled liquid threshold Čerenkov detector; the triggering logic eliminated this pion through NO logic. Though the detection efficiency of this counter was measured in a transmission experiment with $\beta=1$ particles to be $\geq 99.9\%$ efficient, the absolute efficiency to the background pions could not be measured accurately. The further requirement of a delayed coincidence was the final triggering logic line of defense against background.

Protons penetrating to the range parts of the kaon telescope would not, of course, be eliminated by the C_1 detector system because they would generally have low speeds. However, protons with low speeds could not, in first order, be detected by the "decay" Čerenkov detectors, and thus they would not simulate kaon decay.

The counting rates in the different sections of the kaon-telescope were "defined" as pion + proton, and proton, depending on whether the C_1 detector system was turned off or on. These data are summarized in Table IV.

B. Anomalous Sources of Kaons

Production, Target Walls, and Double Scattering

For 1.15-GeV/c pions on liquid deuterium, the source of positive kaons is $\pi^- + d \rightarrow K^+ + \Sigma^- + n$. For a "thick" liquid target, the reactions $\pi^- + d \rightarrow K^0 + \Lambda + n$ and $K^0 + d \rightarrow K^+ + n + n$ are possible but not probable. However, the requirement that all of the events be geometrically reconstructed back to the liquid volume of liquid deuterium eliminates this as a probable cause of background. That is, unless the K^0 's could collide with the walls of the target system, the K^+ yield from this two-stage process is negligible.

The (target empty)/(target full) ratio for kaon-triggered events was $< 1/60$. For other triggering rates see Table IV. Thus, only a negligible fraction of the events could have originated from the walls. The requirement that the reconstructed event originate from the volume of the liquid of the target system reduced this effect to negligible proportions. From an empirical point of view, the fact that the Σ^- mass was measured despite these kinds of background (see Fig. 11) is indicative that they were not serious in the deuterium data.

C. Classification of Scanned Events

All of the data used in the $M(\Sigma^-n)$ missing-mass distribution came from the application of one simple criterion to the kaon-telescope event pictures. Only the $K_{\mu 2}$ decay events in which the heavily ionizing kaon appeared next to the weakly ionizing muon were used. These were called upstream decay events. The only additional visual cut applied to the data was the requirement that only one beam track appear in the beam pion chambers. The geometrical cut applied to the data was that the produced kaon had to originate in the volume of the liquid deuterium.

VI. EXPERIMENTAL RESULTS

Deuterium Target Data

The result is the differential cross section of $\pi^- + d \rightarrow K^+ + \Sigma^- + n$. The differential cross section is determined from the following parameters:

N_K = number of events in the invariant-mass interval $(M, M + \Delta M)$,

N_π = number of pions on the deuterium target,

L = length of deuterium target,

$\Delta\Omega$ = solid angle of the detection system for kaons of energy E_K and angle interval $(\theta_K, \theta_K + \Delta\theta_K)$,

η = detection system's kaon detection efficiency,

N_0 = Avogadro's number.

The experimental differential cross section per target deuteron is

$$\left. \frac{\Delta^2\sigma}{\Delta\Omega\Delta M} \right|_{M, \theta_K} = \frac{N_K(LN_0(\frac{1}{2}))^{-1}}{N_\pi\Delta\Omega\eta\Delta M}. \quad (3)$$

Because of the variation from event to event of the effective values of these parameters and for ease in handling the statistical problem, the experimental differential cross section was determined from the data by determining event by event the effective target length L^i , the effective solid angle $\Delta\Omega^i$, and the effective detection efficiency η^i . Thus the measured differential cross section is

$$\left. \frac{\Delta^2\sigma}{\Delta\Omega\Delta M} \right|_{M, \theta_K} = \frac{(N_0(\frac{1}{2}))^{-1}}{N_\pi\Delta M} \sum_i \frac{(L^i)^{-1}}{\Delta\Omega^i\eta^i} \Big|_{M, \theta_K}. \quad (4)$$

The form the data are finally condensed to is

$$\left. \frac{\Delta\sigma}{\Delta M} \right|_{M, \theta_K} = \frac{(N_0(\frac{1}{2}))^{-1}}{N_\pi\Delta M} \sum_i \frac{(L^i)^{-1}}{\Delta\Omega^i\eta^i} \Big|_{M, \theta_K} \langle \Delta\Omega \rangle_{av}. \quad (5)$$

The sum is over all of the events corresponding to the interval $M, M + \Delta M$ and $\theta_K, \theta_K + \Delta\theta_K$. The calibration of the mass scale of the detection system using the liquid-hydrogen-target events corresponding to reaction (2) at $p_\pi \sim 1.4$ GeV/c was presented in Sec. IV D. The calibration reaction is not used to measure the $\pi^- + p \rightarrow$

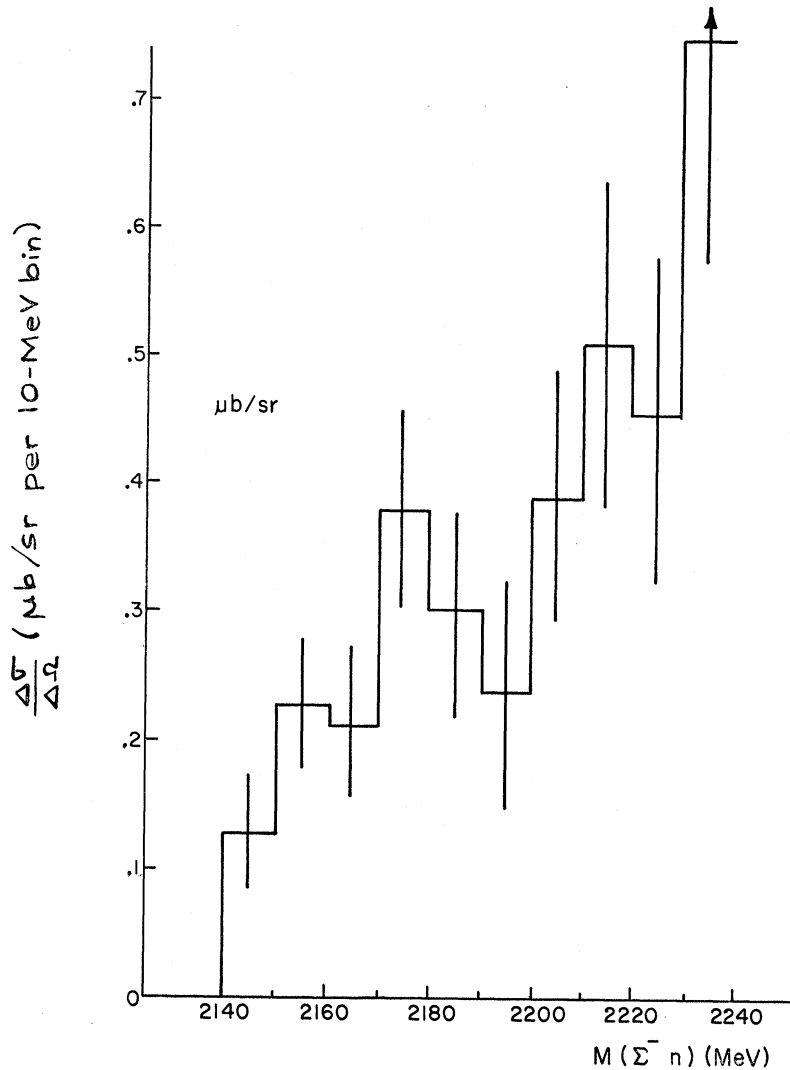


FIG. 12. Differential cross section $d\sigma/dM(\Sigma^-n)$ for the reaction $\pi^- + d \rightarrow K^+ + \Sigma^- + n$ at 1.15 GeV/c. It is determined from the raw data, Fig. 11, and the detector efficiency function, Fig. 9.

$K^+ + \Sigma^-$ differential cross section. The hydrogen-target data calibrated the missing-mass scale and established the fact that the scanning criteria were effective in identifying positive kaons by a direct measurement of the Σ^- mass.

*Measured Differential Cross Section $\Delta\sigma/\Delta M(\Sigma^-n)$
for $\pi^- + d \rightarrow K^+ + \Sigma^- + n$*

All the events from the data reduction in the scanning measuring, Sec. IV D, were analyzed using Eq. (5) and the calculated detection efficiency (Fig. 9) to give the measured differential cross section for the deuterium reaction $\pi^- + d \rightarrow K^+ + \Sigma^- + n$. This result is shown in Fig. 12. The $M(\Sigma^-n)$ mass resolution is 8 MeV; it is assumed to be Gaussian in shape. The kinematical limit on $M(\Sigma^-n)$ is $M_0(\Sigma^-n) = 2137$ MeV. This limit would be the point of "zero binding energy" between the final neutron and Σ^- . Clearly there is no cluster of events at or near M_0 to suggest that a bound $S(\Sigma^-n)$

state exists. These data are used to place an upper limit on the possible $^1S_0(\Sigma n)$ binding energy. The data are also tabulated for the $M(\Sigma^-n)$ distribution in the vicinity of M_0 , Table IX. The systematic errors associated with the data are less than 10% over the M interval of $M_0 - 100$ MeV to $M_0 + 150$ MeV. From the calculated experimental efficiency function (Fig. 9),

TABLE IX. Summary of the corrected data near $M(\Sigma^-n) = M_0(\Sigma^-n) = 2137$ MeV.

$\Delta\sigma/\Delta M^a$ ($\mu\text{b}/\text{sr}$)	M MeV
Zero	2130 - 2140 ^b
0.12 ± 0.04	2140 - 2150 ^b
0.22 ± 0.04	2150 - 2160
0.23 ± 0.036	2160 - 2170
0.38 ± 0.08	2170 - 2180
0.30 ± 0.08	2180 - 2190

^a The errors are statistical. The systematic errors are less than 10% of these statistical errors.

^b There are ten events centered on 2137 MeV within the Gaussian distributed error, 8 MeV of the experimental resolution.

it is seen that the variation of the net efficiency is $\lesssim 3:1$ in this M interval.

VII. CONCLUSIONS

The basic experimental result is the differential cross section for reaction (1), viz., $d\sigma/dM$ as given in Fig. 12 and Table IX. The principal conclusion is that the 1S_0 (Σ^-n) state, if bound, has a BE $\lesssim 0.3$ MeV with a 90% confidence limit. This result is based on an impulse-model used with a final-state interaction model for this possible production process.

A secondary use of these data to determine the 1S_0 (Σ^-n) scattering parameters, scattering length and effective range, does not appear feasible with the present theoretical models.

A. $S(\Sigma^-n)$ Final State Interaction in $\pi^- + d \rightarrow K^+ + \Sigma^- + n$ at 1.15 GeV/c

Several authors have used the impulse approximation in conjunction with a final-state interaction model to describe the possible manifestations of low-energy (Σ^-n) interactions in the associated production of positive kaons.⁶ This model is based on similar work

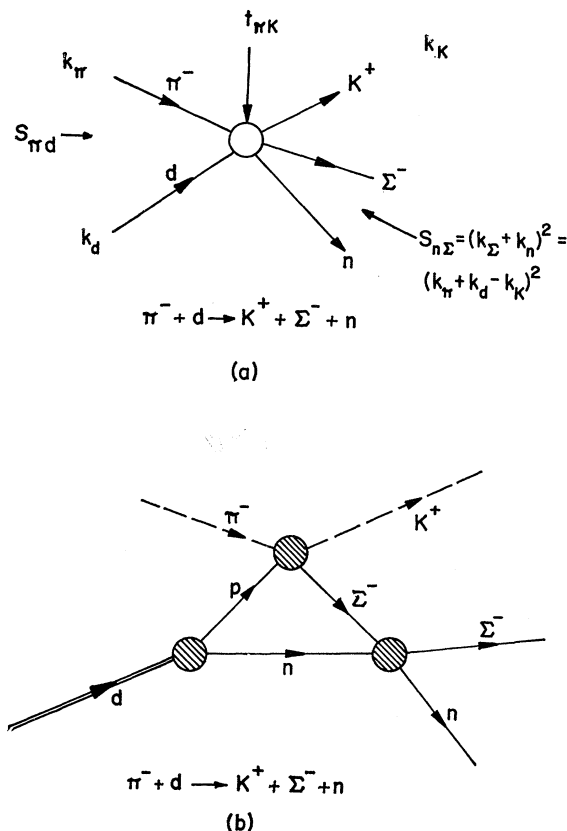


FIG. 13. (a) Kinematical variables of reaction (1). (b) Feynman graph of the impulse production model and final-state interaction model used to describe the reaction $\pi^- + d \rightarrow K^+ + \Sigma^- + n$ phenomenologically.

developed to predict the final-state pion distribution from $\pi^- + d \rightarrow \pi + N + N$ as affected by the final-state nucleon-nucleon interaction.¹¹ The elementary impulse reaction is the associated production of positive kaons from hydrogen $\pi^- + p \rightarrow K^+ + \Sigma^-$.¹² The low-energy (Σ^-n) interaction affects the deuteron-target positive-kaon distribution near 2137 MeV in the (Σ^-n) invariant mass. In the results of this experiment this is the (Σ^-n) missing mass, $M(\Sigma^-n)$, because the (Σ^-n) invariant mass is determined indirectly from the secondary parameters, the pion momentum and the kaon energy and angle, rather than from the measured baryon momenta. See Fig. 13 for the kinematics.

A number of models have been developed to treat this deuteron-target problem.⁶ The Feynman diagram of Fig. 13 depicts the general manner in which the models use the on-the-energy-shell $\pi^- + p \rightarrow K^+ + \Sigma^-$ cross section¹² in conjunction with the final-state interaction terms to describe positive-kaon production from deuterium. If a bound (Σ^-n) state occurs, an enhancement near the mass region $M_0(\Sigma^-n)$ in the (Σ^-n) missing-mass distribution is predicted. With fine enough resolution, the actual binding energy from a possible (Σ^-n) state can be measured. With the 8-MeV resolution of this experiment, the predicted differential cross section $d\sigma/dM$ when compared with the data gives a sensitive determination of a possible 1S_0 (Σ^-n) binding energy. The predicted cross section $d\sigma/dM$ is compared to the data near $M(\Sigma^-n) = M_0(\Sigma^-n) = 2137$ MeV to give an upper limit for the value of the 1S_0 (Σ^-n) BE. The absence of an enhancement in the data of the $M(\Sigma^-n)$ distribution near $M_0(\Sigma^-n)$ is clear evidence for the absence of a bound (Σ^-n) state,⁶ and is, in particular, evidence for the absence of a 1S_0 (Σ^-n) bound state (see Fig. 12).

Theoretical models have been used to predict the differential cross sections for both possible bound states, 3S_1 (Σ^-n) and 1S_0 (Σ^-n). Previous experiments have shown that there is no evidence for a bound 3S_1 (Σ^-n) state.⁴ In positive-kaon production from deuterium with a negative pion beam, the principal manifestation of possible 3S_1 (Σ^-n) final-state interaction occurs for the K 's produced in the forward direction. Forward K 's are necessarily associated with non-spin flip of the target baryon; because the deuteron is primarily 3S_1 , the final-state dibaryon state will also be 3S_1 . Conversely, spin flip of the target baryon is associated with the production of a 1S_0 (Σ^-n) state. Where the maximum sensitivity for the produced 1S_0 (Σ^-n) state occurs in the kaon kinematics is a matter of detailed calculation. However, a simple picture is obtained by considering

¹¹ G. F. Chew, Phys. Rev. **80**, 196 (1950); S. Fernbach, T. A. Green, and K. M. Watson, *ibid.* **84**, 1084 (1951); K. M. Watson and K. A. Brueckner, *ibid.* **83**, 1 (1951); K. M. Watson, *ibid.* **88**, 1163 (1951); G. F. Chew and G. C. Wick, *ibid.* **85**, 1 (1952).

¹² J. C. Doyle, F. S. Crawford, and J. A. Anderson, Phys. Rev. **165**, 1483 (1968); UCRL Report No. UCRL 17703, 1967 (unpublished).

$\pi^-+d \rightarrow K^+(\Sigma^-n)$ as simply $0^-+1 \rightarrow 0^-+1$ with only S and P waves; this leads to the result that the c.m. angular distribution of $d\sigma/d\Omega$ is of the form $A+\sin^2\theta_K$. Thus, to be simultaneously insensitive to 3S_1 (Σ^-n) and sensitive to the manifestations of the possible 1S_0 (Σ^-n) effects, nonforward K 's are measured.

There is the further interesting problem of trying to determine the possible (Σ^-n) scattering length and effective length scattering parameters from the $d\sigma/dM$ cross section. The Hanley and Dante-Henley models⁶ have posed solutions to this problem for the deuteron-target reaction. Attempts to fit the shape of the measured differential cross section to the predicted forms, however, are discouraging in regard to getting meaningful quantitative results. The assumptions and the form of the calculation for the kaon distribution from the (Σ^-n) scattering parameters in the three-body problem $\pi^-+d \rightarrow K^++\Sigma^-+n$ are more complicated than for the two-body problem; i.e., the (Σ^-n) is assumed bound. Further analysis of this problem is being pursued.¹³

B. Limit on 1S_0 (Σ^-n) BE from Differential Cross Section $\Delta\sigma/\Delta\Omega|_{M(\Sigma^-n)}$

The data giving the differential cross section $\Delta\sigma/\Delta\Omega$ (see Fig. 12) are examined at the kinematical limit $M_0(\Sigma^-n)=2137$ MeV. It is clear there is no significant enhancement of events at or near this "zero-binding-energy" region of $M(\Sigma^-n)$. In fact, the data "cut off" rather sharply at approximately this theoretical limit. There are ten corrected events in the region $M_0(\Sigma^-n)$ for the 8-MeV experimental resolution, assuming the resolution function is Gaussian in shape. In fact, the final data, Fig. 12, "cut off" rather sharply at approximately this theoretical limit. There were seven events in the region $M(\Sigma^-n)=2137$ MeV within the experimental resolution; there are ten events within a 90% confidence limit on this sample. The composite experi-

mental detection efficiency is 0.072 cm sr (Fig. 9), there were 1.9×10^{10} pions incident on the liquid-deuterium target. Thus, there is a cross section $\sigma \leq 0.16 \mu\text{b sr}^{-1}$, 90% confidence, for $\pi^-+d \rightarrow K^+(\Sigma^-n)$ at 1.15 GeV/c, $25^\circ \leq \theta_{K \text{ lab}} \leq 60^\circ$. From the results of the Dante-Henley model, this corresponds to a binding energy of 0.3 MeV with a 90% confidence limit. Thus, having a binding energy of less than 0.3 MeV, the 1S_0 (Σ^-n) state is weakly bound, if bound at all.

There are several theoretical models dealing with the possible hyperon-nucleon interactions.³ None of them seems to be sufficiently well developed to make predictions about all of the possible physical hyperon-nucleon states. The situation now seems to be waiting on the measurement of most of the dibaryon states before the complete structure of the different $SU(3)$ states can be understood. An example of the kinds of difficulties is the very large effect of mass differences between the different baryons. If, for example, a calculation indicated that the (Σ^-n) state were strong enough to be bound with zero binding energy for $M_{\Sigma^-}=M_n=939$ MeV, then simply putting in the additional kinematical fact that M_{Σ^-} is actually 1197 MeV would increase the effective potential-well depth by ~ 1.13 , and thus induce a considerable binding energy.

ACKNOWLEDGMENTS

The authors wish to thank D. Jauch, N. Sossong, L. Bond, and H. Spore for their assistance in the preparations and in the data taking. O. Sander's assistance in the running was appreciated. They want to thank the numerous scanners and measurers who followed through the painstaking work of extracting the data from the film. Appreciation for their interest in many stages of this work is extended to Dr. R. W. Williams, Dr. E. Henley, and Dr. M. Dante. One of us (HD) wants to thank Dr. R. Dalitz and Dr. R. Warnock for the early interest they showed in this method of studying hyperon-nucleon interactions. Finally, we want to thank the staff, technical and service, at the Brookhaven National Laboratory for their hospitality.

¹³ H. F. Davis, *Lectures in Theoretical Physics* (Gordon & Breach, New York, 1969), Vol. 11, B, Pt. 2.